Sgs1^{BLM} independent role of Dna2^{DNA2} nuclease at DNA double strand break is inhibited by Nej1^{XLF}

Aditya Mojumdar, Nancy Adam, and Jennifer A. Cobb*

Departments of Biochemistry & Molecular Biology and Oncology, Robson DNA Science Centre, Arnie Charbonneau Cancer Institute, Cumming School of Medicine; University of Calgary; 3330 Hospital Drive N.W., Calgary, AB T2N 4N1, Canada.

* Lead Contact: Tel.: +1 403 220 8580 or Email: jcobb@ucalgary.ca

Short Title: Interplay of Nej1 with Sae2 and Dna2 nuclease at DSB

Keywords: DSB repair, Repair pathway choice, Nej1, Sae2, Dna2, 5' resection, end-bridging

Abstract

The two major pathways of DNA double strand break (DSB) repair, non-homologous end-joining (NHEJ) and homologous recombination (HR), are highly conserved from yeast to mammals. Regulated 5' DNA resection is important for repair pathway choice and repair outcomes. Nej1 was first identified as a canonical NHEJ factor involved in stimulating the ligation of broken DNA ends. More recently, Nej1 was shown to be important for DNA end-bridging and inhibiting Dna2-Sgs1 mediated 5' resection. Here, we show Nej1 interacts with Sae2, which inhibits Dna2-Sae2 mediated 5' resection and Dna2 recruitment to the DSB in the absence of Sgs1. The synthetic lethality of *sae2*Δ *sgs1*Δ is reversed by the deletion of *NEJ1* and is dependent on the nuclease activity of Dna2, but not Exo1. By contrast, Nej1 and Sae2 function together in bridging the DNA ends, an event that does not directly involve Sgs1 or Dna2. We demonstrate the importance of Nej1 interactions with Sae2 in these two key events that impact repair pathway choice, 5' resection and end-bridging, which provides insight for how Nej1 prevents genomic deletions from developing during DSB repair.

Author summary

The core NHEJ factor Nej1 regulates double-strand break (DSB) repair through its inhibitory interactions with multiple factors that are central to 5' DNA resection at the break . Nej1 not only inhibits resection mediated by Dna2-Sgs1, but it inhibits Dna2 localization to the DSB through an Sgs1-independent mechanism involving Sae2. Nej1 interacts with Sae2 to promote end bridging and to inhibit the initiation 5' DNA resection by Sae2-Dna2.

Introduction

DNA double-strand breaks (DSBs) can be repaired by two central pathways, non-homologous end joining (NHEJ) and homologous recombination (HR). NHEJ mediates the direct ligation of DNA ends without the requirement for end processing, whereas HR requires 5' end resection. Both 5' resection and end-bridging are important for repair pathway choice and down-stream DNA processing. Once resection initiates at a DSB, repair by canonical NHEJ is no longer an option. A network of proteins, involving the core NHEJ factor Nej1, has evolved to regulate this key step [1-9].

yKu70/80 (Ku) and Mre11-Rad50-Xrs2 (MRX) are the first complexes that localize to a DSB and both are important for recruiting Nej1 [1-4]. Cells lacking *NEJ1* are as defective in end-joining repair as *ku70*Δ and *dnl4*Δ [3, 5, 6]. Nej1 contributes to Ku stability, which protects the DNA ends from nucleolytic degradation, and promotes Lif1-Dnl4 mediated ligation [2, 3, 7, 8]. Nej1 also functions in collaboration with MRX in DNA end-bridging. The structural features of the MRX complex are critical for end-bridging and deletion of *NEJ1* result in end-bridging defects that are additive with *rad50* mutants [4, 10-13].

While Nej1 and MRX both contribute to DNA end-bridging, Nej1 functions antagonistically to MRX by inhibiting 5' DNA resection. 5' DNA resection occurs through a two-step process [14]. First, Sae2, the yeast homologue of human CtIP, interacts with Mre11 endonuclease initiating DNA resection and promoting Ku dissociation from the DNA ends [15, 16]. Second, Dna2 and Exo1, two functionally redundant 5' to 3' nucleases, drive long-range resection [16, 17]. Mre11 endonuclease activity is less critical for 5' resection than the physical presence of the MRX complex. Both long-range nucleases, Dna2, in complex with Sgs1 helicase, and Exo1, require MRX for localization and can serve as compensatory back-ups to initiate resection, albeit with delayed kinetics, in the absence of Mre11 nuclease activity [9, 17, 18]. Few mechanistic details exist for how Nej1 inhibits 5' resection, however the role of Nej1 in DSB pathway choice involves more than just reinforcing Ku-dependent DNA end protection as previously described for NHEJ. Moreover, the interplay of Nej1 with the long-range nucleases, Dna2-Sgs1 or Exo1, is

distinct [4, 9]. Nej1 and Exo1 appear to function independently of one another. For example, Exo1 has a very high affinity for DNA ends that are not protected by Ku and it can initiate resection in *mre11* nuclease dead (nd) mutants only when *KU70* is deleted, but not when *NEJ1* was deleted [19, 20]. By contrast, Nej1 inhibits Dna2 and the hyper-resection of *nej1*Δ mutants is Dna2 dependent and Exo1 independent [4, 9].

The regulation of Dna2 in resection is likely more complex than that of Exo1, which largely depends on whether Ku is binding the DNA ends. In the absence of Sae2 or Mre11 activity, resection initiates primarily through Dna2, independently of *KU* status [21-23]. Dna2 and Mre11 show functional redundancy for processing the ends of DSBs after radiation treatment [24]. Even though previous work showed that Dna2 can serve as a back-up when Mre11 is compromised, it did not exclude a potential role for Dna2 in initiating resection in *MRE11*+ cells.

Dna2 is mutated in a myriad of human cancers but understanding its entire function at DSBs has been challenging because *DNA2* is an essential gene involved in Okazaki fragment processing, therefore it cannot be deleted [25-29]. Earlier work showed that the lethality of *dna2*Δ can be supressed by disruption of *PIF1* helicase [30]. The rate of 5' resection decreased at a DSB in *dna2*Δ *pif1*-m2 mutants, but not further in triple mutants where *SGS1* was also deleted [19].

The epistatic relationship for *DNA2* and *SGS1,* and the inefficiency of Dna2 helicase activity, supported a model whereby Dna2 and Sgs1 function together as complex in long-range resection [16, 31]. Subsequently, deletion of *SGS1* has been used as a surrogate for describing Dna2 functionality at DSBs. However, these data do not account for the greater IR and UV sensitivity of *dna2*-1 *sgs1*Δ mutants compared to single mutant counterparts, with the nuclease deficient allele *dna2*-1 (P504→S) showing greater sensitivity than *sgs1*Δ [32]. Indeed, all work points to an important role for Dna2 in 5' resection, however, there remains a gap in understanding Dna2 regulation and functionality in DSB repair. Sae2 was recently shown to stimulate the nuclease and helicase activity of Dna2-Sgs1, although this needs to be demonstrated *in vivo* at the break site [33, 34]. Moreover, the relationship between Nej1 and Sae2 also needs investigating because, like MRX and Nej1, Sae2 has a role in DNA end-bridging at DSBs [35], a function conserved in humans and with Ctp1 in fission yeast [36, 37].

In the current work we demonstrate that Nej1 functions in opposition to Dna2 and Sae2 in DNA end processing at DSBs. In *sae2*Δ and nuclease deficient *dna2*-1 mutants, the recovery of Nej1 at the break and the frequency of NHEJ repair increase, whereas the deletion of *NEJ1* leads to an increased rate of 5' resection and increased recovery of Dna2 and Sae2 at the break. We show that Sae2 is a key factor in Dna2 recruitment to DSBs. Nej1 binds with Sae2, inhibiting its physical association with both Dna2 and each component of the MRX complex. However, unlike deleting *SAE2* or *EXO1* or disrupting the nuclease activity in *mre11*-3, we found no compensatory back-up for the loss of Dna2 nuclease activity in 5' resection at DSBs. Consistent with this, the 5' resection defect in *dna2*-1mutants was more penetrant than in *sae2*Δ or *sgs1*Δ, even when the inhibition by Nej1 was removed. In general, deletion of *NEJ1* did not increase 5' resection in cells harboring the *dna2*-1 allele. Moreover, large genomic deletions that develop in *nej1*Δ as a result of hyper-resection were only reversed when combined with *dna2*-1, and not by deleting *SAE2*, *SGS1*, or by disrupting the nuclease activity with *mre11-3 or exo1*Δ mutations. Aside from regulating 5' resection, Nej1-Sae2 interactions might be functionally important for end-bridging as deletion of both *NEJ1* and *SAE2* showed epistatic defects. Lastly, we show that deletion of *NEJ1* can reverse the synthetic lethality of *sae2*Δ *sgs1*Δ through a mechanism dependent on the nuclease activity of Dna2.

Results

Sgs1-independent recruitment of Dna2 nuclease is inhibited by Nej1

The core NHEJ factor Nej1 has been shown to inhibit Dna2-Sgs1 dependent 5' DNA resection at DSBs [4, 9]. Deletion of *SGS1* reverses hyper-resection in *nej1*Δ mutants and it also decreases the frequency of large genomic deletions that form at a DSB. To determine whether the loss of Dna2 nuclease activity resulted in similar phenotypes, we combined nuclease dead *dna2*-1 with *nej1*Δ [25, 26]. 5' DNA resection was measured at the HO-induced DSB using a quantitative PCR-based approach developed by others and previously used by us [4, 9, 35, 38]. It relies on an *Rsa*I cut site located 0.15 kb from the DSB (Fig 1A). If resection has proceeded past the cut site, the single-stranded DNA is produced which will be amplified by PCR. 5' resection was reduced

more in *dna2*-1 mutants compared to *sgs1*Δ, and the rate in *dna2*-1 *nej1*Δ double mutants remained below wild type and *sgs1*Δ *nej1*Δ (Fig 1B). We next determined Dna2 localization to the HO-DSB by performing chromatin immuno-precipitation (ChIP) with primers located 0.6 kb from the break, between the *MATα1* and *MATα2* genes (Fig 1A). The recovery of Dna2 was similarly compromised in *sgs1*Δ and *dna2*-1 mutant cells (Fig 1C), however Sgs1 recruitment remained at wild type levels in *dna2*-1 (Fig S1A). Consistent with previous reports, Dna2 recruitment to a DSB increased in *nej1Δ* (Fig 1C) [4]. Dna2 was also recovered at a DSB independently of Sgs1 with a reduction compared to wild type, but well above the non-tagged (NT) control. Interestingly, this Sgs1-independent pathway of Dna2 recruitment was inhibited by Nej1 as its recovery at the DSB was similar in *sgs1*Δ *nej1*Δ and *nej1*Δ mutants (Fig 1C). We also determined the inverse correlation. ChIP on Nej1 at the DSB showed an increase in recovery at the DSB in *dna2*-1 compared to in wild type cells (Fig S1B). This is consistent with previous work where Dna2 overexpression resulted in decreased Nej1 localization [4], underscoring the antagonistic relationship between Nej1 and Dna2. By contrast, Nej1 levels were only mildly reduced in *sgs1*Δ mutants, which is notable given Nej1 physically interacts with Sgs1, but not Dna2 [4].

End-joining as determined by cell survival on continuous galactose inversely correlates with 5' DNA resection. Cell survival increases in *sgs1*Δ and even more so in *dna2*-1 mutants (Fig 1D). However, Nej1 is essential for end-joining and growth on galactose was markedly reduced in all mutant combinations containing *nej1*Δ (Fig 1D). Overall, compared to transient galactose exposure [8, 9], the rates of survival are very low with continuous exposure because only cells that have acquired mutations, which prevent recutting can survive (Table S1). Determining the mating type of the survivors provides a physiological readout of DNA processing events and genomic alterations occurring at the HO-DSB, which is located within MATα1 and adjacent to MATα2 (Fig 1E). Expression of these genes regulates the mating type by activating α -type genes and inhibiting a-type genes. Extensive resection leads to large deletions (>700 bp) and when both α1 and α2 genes are disrupted, a-like survivors are produced (red). Small deletions or insertions lead to sterile type survivors (blue) and repair events resulting in α-type survivors show no sequence change at the HO recognition site (Fig 1E). Consistent with previous reports,

in WT cells and *sgs1*Δ mutants, the majority of survivors are sterile (blue), and contain small insertions or deletions (Fig 1F) [9, 39]. By contrast, of the *dna2*-1 survivors, which is < 1% (Fig 1D), most were α-type (gray) without mutation in the HO recognition sequence. Early work indicates that α-type survivors after DSB induction repair through canonical NHEJ, and survive because re-cleavage is disrupted by defects in the HO endonuclease [39]. Of note, the increased survival and α-mating type in *dna2*-1 mutants (Fig 1D and 1F) did not result from defects in DSB formation as cut efficiency was similar to wild type 2 hours after galactose induction (Table S1).

Dna2 recruitment to DSB is independent of Exo1

We next determined Sgs1-independent 5' resection and Dna2 recovery when the other nucleases were disrupted, using *mre11*-3 nuclease dead or *EXO1* deletion. While *mre11*-3 disrupts nuclease activity, the complex localizes to the DSB similarly in *MRE11*+ and *mre11*-3 mutants [40, 41]. This is important because the presence of MRX is necessary for the recruitment of all the processing factors we are investigating at the DSB, including Nej1 and the long-range resecting factors, Exo1 and Dna2-Sgs1.

Consistent with previous reports, 5' resection in *mre11*-3 and *exo1*Δ were indistinguishable from wild type (Fig 2A and 2B) [9]. The rates of 5' resection in *mre11*-3 *dna2*-1 and *exo1*Δ *dna2*-1 double mutants were severely reduced compared to double mutant combinations with *sgs1*Δ (Fig 2A, 2B and 1B). Deletion of *NEJ1* modestly rescued the resection defect in *exo1Δ sgs1*Δ and *exo1*Δ *dna2*-1 (Fig 2B). However, the 5' resection pattern was very different in *mre11*-3 triple mutant combinations, which remained low in *mre11*-3 *dna2*-1 *nej1*Δ, but in *mre11*-3 *sgs1*Δ *nej1*Δ was indistinguishable from wild type (Fig 2A). Furthermore, while resection was equally abrogated in *mre11*-3 *dna2*-1 and *mre11*-3 *dna2*-1 *nej1*Δ, and below *mre11*-3 *nej1*Δ, survival on galactose correlated directly with *nej1*Δ and was markedly down in all mutant combinations where *NEJ1* was deleted (Fig 2C). These data underscore the importance of Nej1 in end-joining independently of 5' resection status. Survival of *mre11*-3 *dna2*-1 cells was above *mre11*-3 and wild type, which is consistent with resection being inversely correlated with survival (Fig 2C). Survival increased slightly more in double mutant combinations with *dna2*-1 compared to double mutant combinations with *sgs1*Δ (Fig 2C), however the types of survivors that

developed between the two groups were different. Survivors with *SGS1* deletions, *mre11*-3 *sgs1*Δ and *exo1*Δ *sgs1*Δ, were primarily sterile with small indels (blue, Fig 2D). By contrast, survivors harboring *dna2*-1 showed an increase in non-mutagenic NHEJ (gray) and no large deletions (red) in triple mutant combinations where *NEJ1* was also deleted, as seen when comparing *mre11*-3 *sgs1*Δ *nej1*Δ and *mre11*-3 *dna2*-1 *nej1*Δ (Fig 2D).

To determine whether 5' resection and HO survival differences in *mre11*-3 and *exo1*Δ were related to Dna2 localization +/- *SGS1* status, ChIP was performed on Dna2 in the different mutant combinations. Deletion of *NEJ1* increased the recovery level of Dna2 at the break in all mutant backgrounds (Fig 2E). Consistent with our earlier work, Nej1 and Exo1 function independently of each other [9]. Deletion of *EXO1* did not alter Dna2 protein levels recovered at the DSB in otherwise wildtype or *nej1*Δ mutants, which is consistent with the 5' resection data where rates in *exo1*Δ and *exo1*Δ *nej1*Δ mutants were similar to wild type and *nej1*Δ respectively (Fig 2B and 2E). Even though the rate of resection was lower in *exo1*Δ *sgs1*Δ mutants compared to *sgs1*Δ, the level of Dna2 recovered was similar (Fig 2E and 1C). By contrast, the recovery of Dna2 in *mre11*-3 *sgs1*Δ was higher than in *sgs1*Δ (p-value < 0.05), and similar to wild type (Fig 2E and 1C). Overall, these data suggest that Sgs1-independent recruitment of Dna2, which is inhibited by Nej1, involves a factor linked to Mre11 nuclease activity. This led us to investigate a potential role for Sae2, which was recently shown to increase at the DSB in *mre11*-3 mutants [22].

Sae2-dependent recruitment of Dna2 is inhibited by Nej1

Sae2 interacts with the MRX complex to activate Mre11 endonuclease and more recently it was also shown to stimulate the nuclease activity of Dna2 [16, 33, 34]. While Sae2 recruitment to the DSB is abrogated in *mre11*Δ mutants, by ChIP localization increased in *mre11*-3 (Fig 3A) [22]. Thus, we determined whether Dna2 localization to the DSB in *mre11*-3, which was similar to wild type (Fig 2E), depended on Sae2. Indeed, the recruitment of $Dna2^{HA}$ significantly decreased in *mre11-3 sae2*Δ and *sae2*Δ mutant cells (Fig 3B). Furthermore, the increased recovery of Dna2 in *mre11*-3 *nej1*Δ double mutants was Sae2 dependent (Fig 2E and 3B). Interestingly, by ChIP Dna2 recovery was lower in *sae2*Δ *nej1*Δ compared to *sgs1*Δ *nej1*Δ (Fig 1C

and 3B). Furthermore, in the course of our investigation, we observed Sae2 localization also increased in *nej1*Δ (Fig 3A). The increase was additive with *mre11*-3, with Sae2 recovery being higher in *nej1*Δ *mre11*-3 than either single mutant (Fig 3A). Conversely, Sae2 recovery in *dna2*-1, and both *sgs1*Δ and *exo1*Δ mutants, remained indistinguishable from wild type (Fig S1D and S1E).

These ChIP data indicate that Sae2 recruitment, and Sae2-dependent recruitment of Dna2, are regulated by Nej1, prompting us to determine the interactions between these factors and their impact on 5' DNA resection at the break site. Deletion of *SAE2* reversed the hyper 5' resection of *nej1*Δ mutants (Fig 3C), thus the presence of Nej1 at DSBs likely inhibits resection in part by regulating Sae2 localization. This was not an indirect consequence of disrupting NHEJ repair in general because in contrast to *nej1*Δ, Sae2 recovery by ChIP at the DSB did not increase when either *DNL4* or *KU70* were deleted (Fig S1D).

We determined whether the interplay between these factors involved physical interactions. Yeast-two-hybrid (Y2H) was performed as previously described with prey vector HA-tagged Sae2 expressed together with the following bait vectors: LexA-tagged Nej1, MRX subunits, or Dna2 domains - 1-450 aa (N-term), 451-900 aa (nuclease) and 901-1522 aa (helicase) as previously described [4, 42]. All constructs were regulated by galactose-induction and expressed similarly in WT and *nej1*Δ backgrounds (Fig S2A). Consistent with previous reports [43], Sae2 physically interacts with the MRX complex (light blue bars, Fig 3D). Sae2 also shows robust binding with Nej1 (red bar) and interacts with the N-terminal regulatory region and nuclease domains of Dna2 (light green bars). Interestingly, Sae2-Dna2 and Sae2-MRX interactions increased in *nej1*Δ mutants (dark blue and green bars, Fig 3D). This was similar to previous Y2H observations where both Dna2-Sgs1 and Dna2-Mre11 interactions increased when *NEJ1* was deleted [4]. Of note, deletion of *NEJ1* did not increase general binding between all proteins expressed from 2-hybrid vectors as Mre11-Rad50 interactions were unaltered in *nej1*Δ cells (Fig S2B). Taken together with previous work [4], the presence of Nej1 inhibits interactions between nucleases and nuclease regulators. In addition to Nej1 inhibiting the

binding of Sgs1-Dna2 and Mre11- Dna2 [4], it also physically interacts with Sae2 inhibiting both MRX-Sae2 and Sae2-Dna2 binding.

Similar to *dna2*-1, the rate of survival and non-mutagenic end-joining increased in *sae2Δ* mutants (Fig 4A). However, unlike *dna2*-1, large deletion developed when *sae2*Δ was combined with *nej1*Δ (Fig 1E and 4B). We previously showed that large deletions at the DSB develop through a combination of defects in 5' resection and DNA end-bridging [4]. End-bridging was measured in cells where both sides of the DSB are tagged with fluorescent markers. The TetO array and the LacO array were integrated 3.2 Kb and 5.2Kb respectively from the DSB in cells expressing $TetR^{GFP}$ and $LacO^{mCherry}$ fusions, enabling us to visualize both sides by fluorescence microscopy (Fig 1A and 4C). In asynchronous cells, the distance between the GFP and mCherry foci was measured prior to (0 hr) and after (2 hr) DSB induction. In wild type cells, the distance between the fluorescent markers did not show a significantly different mean distance after HO cutting (0.28 µm) compared to before galactose induction (0.24 µm), indicating successful DNA end-bridging at the break (Fig 4D). The distance between markers increased in *sae2Δ* mutant cells (0.44 µm), indicating a defect in end-bridging (Fig 4D). However, no significant increase was observed after DSB induction in *dna2*-1, *sgs1*Δ, or *exo1*Δ mutants (Fig S3).

A comparison between *mre11*-3 and *sae2*Δ +/- *NEJ1* in 5' resection and end-bridging supports the model that both processes safeguard against the development of large deletions. In *mre11*-3 mutants, 5' resection proceeded but end-bridging was not disrupted, whereas in *sae2*Δ mutants, bridging was disrupted but 5' resection was low and neither single mutant showed large deletions (Fig 3C, 4B and 4D). By contrast, large deletions formed when both mutants were combined with *nej1*Δ. The end-bridging defect in *sae2*Δ mutants was epistatic with *nej1*Δ, yet the rate of 5' resection increased in *sae2*Δ *nej1*Δ compared to *sae2*Δ, and large deletions also formed. Moreover, *mre11*-3 *nej1*Δ and *mre11*-3 *sae2*Δ had similar end-bridging defects, however both 5' resection and Dna2 levels remained low and large deletions did not develop in *mre11*-3 *sae2*Δ survivors. Taken together, our data support a role for Sae2, together with Nej1, in end-bridging and also a role for Sae2-Dna2 in 5' resection at the DSB, a pathway inhibited by Nej1 distinct of Sae2 activation of Mre11 endonuclease (Fig 4D).

Dna2 plays a major role in resection at DSB that is inhibited by Nej1

We observed that recruitment of Dna2 to DSBs was partially dependent on Sae2 and Sgs1, and both pathways were inhibited by Nej1. Furthermore, the rate of resection was severely hampered in cells harboring the *dna2*-1 mutation, which was modestly alleviated by *NEJ1* deletion. These data indicate that both Dna2 levels and its nuclease activity were important for DNA processing at DSBs, prompting us to determine whether *nej1*Δ, which removes Dna2 inhibition, would alleviate *sae2*Δ *sgs1*Δ synthetic lethality (SL) [22]. We crossed *sae2*Δ *nej1*Δ with *sgs1*Δ *nej1*Δ and spores with the triple mutant combination grew remarkably well (Fig 5A). The triple mutants showed a low level of survival, similar to other mutant combination containing *nej1*Δ, and an accumulation of large deletions under chronic HO induction (Fig 5B and 5C). The rate of resection in the triple mutant was indistinguishable from wild type and significantly higher than levels in *sae2*Δ and *sgs1*Δ single mutants (Fig 5D). Moreover, $Dna2^{HA}$ recruitment to a DSB in *sae2*Δ *sgs1*Δ *nej1*Δ mutants was similar to WT (Fig 5E), and above levels in *sae2*Δ +/- *NEJ1* or *sgs1*Δ (Fig 1C and 3B). To determine whether suppression of *sae2*Δ *sgs1*Δ lethality by *NEJ1* deletion required Dna2 nuclease activity, we generated heterozygous diploids for *sae2*Δ *sgs1*Δ *nej1*Δ and *dna2-1* and upon tetrad dissection recovered no viable spores with the quadruple mutant combination (Fig 5F). By contrast, *sae2*Δ *sgs1*Δ *nej1*Δ *exo1*Δ spores were viable, thus suppression of *sae2*Δ *sgs1*Δ synthetic lethality by *nej1*Δ depends on the nuclease activity of Dna2, not Exo1 (Fig S4). Taken together, our data support a model whereby Dna2 is recruited to a DSB through three pathways, which are all under inhibition by Nej1 (panel (a); Fig 5G). Dna2 localizes primarily through binding with Sae2 and Sgs1, thus deletion of both results in lethality (panel (b); Fig 5G). Removal of Nej1, which binds Mre11-C , allows Dna2 recruitment through Mre11-Dna2 interactions [4]. Initial resection and cell viability in *sae2*Δ *sgs1*Δ *nej1*Δ triple mutants is Dna2 dependent. However, when Ku dissociates, Exo1 nuclease would be more efficient, especially for long-range resection in cells where *SGS1* has been deleted (panel (c); Fig 5G).

Discussion

Here we show Nej1 to be a general inhibitor of 5' resection mediated by Dna2, which is recovered at DSBs through interactions with Sae2, independently of Sgs1. Nej1 inhibits Sae2-dependent Dna2 localization and the localization of Sae2 itself to the DSB. Nej1 physically interacts with Sae2, and our data support a model whereby Nej1-Sae2 interactions inhibit Sae2 binding with MRX and Dna2, which down-regulates 5' DNA resection. However, deletion of *NEJ1* and *SAE2* show epistatic end-bridging defects, raising the possibility that Nej1 and Sae2 also collaborate mechanistically to restrain the broken DNA ends at the DSB (Fig 4D and 4E).

Sae2-dependent recruitment of Dna2 is inhibited by Nej1

Dna2 localization to the break is only partially governed by Sgs1 (Fig 1C). Consistent with previous findings, the alternative mode of Dna2 recruitment involves Sae2 (Fig 3B; [19]). Our findings differ slightly from previous work, which showed Dna2 is reduced at 2 hours, but not at 3 hrs, in *sae2*Δ mutant cells [19]. This discrepancy could result from slight variations in experimental design because in the same study Ku70 was not altered 3 hrs after HO induction in *sae2*Δ mutants, yet we find that Ku70 levels increase slightly (Fig S1C). Our results are in line with earlier work showing that the damage sensitivity of *sae2*Δ is suppressed by *KU70* deletion as well as previous work in S. *pombe* where *ctp1*Δ mutants show increased Ku70 levels at DSBs [20, 41, 44]. Moreover, our data support previous work showing a role for human CtIP in Dna2 recruitment to DSBs [45], and also provide a physiological framework for *in-vitro* studies where CtIP was shown to have a stimulatory effect on Dna2 nuclease [33, 34].

When *NEJ1* was deleted in *sgs1*Δ mutants, Dna2 recovery by ChIP increased above levels recovered in wild type cells, indicating that the Sae2 dependent pathway might also be inhibited by Nej1 (Fig 1C; [4]). Indeed, our data support this model as physical interactions between Sae2 and Dna2 increased in *nej1*Δ mutant cells (Fig 3D). Furthermore, Dna2 enrichment levels at DSBs also correspond to resection levels in the various mutant backgrounds, all of which were *SGS1*+ (Fig 3B and 3C), suggesting 5' resection mediated by Sae2-dependent recruitment of Dna2 to DSBs was also regulated by Nej1.

MRX is required for the recruitment of all these processing factors to the DSB, thus *mre11*-3 was used in this study because although this allele is nuclease dead, the complex recruits to the break site [12, 13]. There was a marked decrease in Dna2 in *sae2*Δ mutant cells compared to *mre11*-3 (Fig 2E and 3B). Dna2 recruitment did increase in *sae2*Δ *nej1*Δ, compared to *sae2*Δ mutants, however recovery remained below levels in *mre11*-3 *nej1*Δ mutants (Fig 2E and 3B). These differences might be related to checkpoint signalling defects in *sae2*Δ mutants, defects that are independent of Mre11 nuclease activity [22]. Moreover, even though our data do not contradict the role of Sae2 as a nuclease [23], further studies involving Nej1, Dna2 with Sae2-mutants (D285P/K288P and E161P/K163P) is certainly warranted.

Nej1 and Sae2 in end-bridging

Nej1 physically interacts with Sae2 and down-regulates Sae2 interactions with MRX. Consistent with earlier work, Sae2 has a role in end-bridging (Fig 4D; [35-37]). However, in contrast to the additive end-bridging defects for *rad50*Δ *nej1*Δ [4], *sae2*Δ end-bridging defects are epistatic with *nej1*Δ. Given the physical interaction between Nej1 and Sae2 (Fig 3D), it is possible that the two factors could function as a complex in end bridging. It might be informative to determine whether Sae2 and Nej1 can form hetero-oligomers, distinguishing a sub-population of Sae2 involved in DNA end-bridging apart from Sae2 homo-oligomers involved in Mre11 activation and checkpoint signalling [46, 47]. Importantly, none of the other factors involved in 5' resection showed an end-bridging defect when disrupted including *exo1*Δ, *sgs1*Δ, or *dna2*-1 (Fig S3). DNA end-bridging was also maintained in *mre11*-3 mutants, which is in line with previous work showing that the structural integrity of the MRX complex, but not its nuclease activity, is important for bridging [12, 13, 48].

The relationship between Dna2 and NHEJ factors

Our data also suggest that Dna2 and Nej1 have an antagonistic relationship rather than a unidirectional one where Nej1 inhibits Dna2. End-joining repair rates increase in cells harbouring the *dna2*-1 mutation. Consistent with this, the recovery of Nej1 and Ku70 by ChIP also increase at DSBs in *dna2*-1 (Fig S1B and S1C), suggesting end-joining is promoted in part

because 5' resection is delayed. With the exception of Ku, mechanistic understanding about how NHEJ factors contribute to repair pathway choice remains fairly obscure. The interplay between these factors is complex as Ku is important for Nej1 recruitment, and in turn, Nej1 stabilize Ku. However, in *nej1*Δ cells, Ku still provides end-protection and the deletion of *NEJ1* has different genetic requirements for inhibiting resection compared to those previously identified for the deletion of *KU70* [4, 9] . For example, deletion of either *KU70* or *NEJ1* can suppresses the 5' resection defect and damage sensitivity of *mre11*-3 mutants (Fig 2A; [20, 41]), however the rescue of *mre11*-3 by *ku70*Δ depends on Exo1 whereas the rescue by *nej1*Δ is Exo1-independent [4, 9, 41]. Nej1, by contrast, regulates resection mediated by Dna2 and Dna2-dependent resection initiates independently of *KU* status [4, 9, 21-23].

The 5' resection defects in *dna2*-1 mutants support a role for Dna2 in DSB repair independently of Sgs1. Even though Dna2 levels were similarly reduced in *dna2*-1 and *sgs1*Δ, 5' resection was more defective in *dna2*-1 mutants. Dna2 and Sgs1 have important links to the DNA damage checkpoint [49], however the greater resection defect in *dna2*-1 is likely not attributed to its checkpoint functions as mutations in Dna2 that disrupt signalling map to its N-terminal region, distinct of its nuclease and helicase activities [50]. Double mutant combinations involving *EXO1* deletion with either *dna2*-1 or *sgs1*Δ also support an Sgs1-independent function for Dna2 at the DSB. 5' resection was markedly reduced in both *exo1*Δ *dna2*-1 and *exo1*Δ *sgs1*Δ, however deletion of *NEJ1* reversed the resection defect more in *exo1*Δ *sgs1*Δ *nej1*Δ than *exo1*Δ *dna2*-1 *nej1*Δ triple mutants (Fig 2B). Although resection did increase in *exo1*Δ *dna2*-1 *nej1*Δ compared to *exo1*Δ *dna2*-1, this was independent of *EXO1*, as resection rates were indistinguishable from *dna2*-1 *nej1*Δ and *dna2*-1 respectively (Fig 1B and 2B). Further support for Sgs1-independent functions of Dna2 at DSBs comes from assessing repair outcomes. The *dna2*-1 survivors contained very few mutations at the break site whereas *sgs1*Δ survivors contained a high percentage of small indels, indicative of some short-range resection (Fig 1F). These repair outcomes were unaltered by the further deletion of EXO1, as *exo1*Δ *dna2*-1 and *exo1*Δ *sgs1*Δ survivors were comparable to their single mutant counterparts, and *exo1*Δ survivors had a high percentage of small indels like *sgs1*Δ (sterile mating type) (Fig 1F and 2C). By contrast, *nej1*Δ

double mutant combinations led to large deletions in *sgs1*Δ *nej1*Δ and *exo1*Δ *nej1*Δ, but not in *dna2*-1 *nej1*Δ mutants (Fig 1F and 2C).

Of note, *exo1*Δ *dna2*-1 double mutants were also viable, which contrasts the lethal interaction previously reported for *exo1*Δ *dna2*Δ *pif1*-m2 [17]. How the *pif1*-m2 mutation might impact the genetic interaction between *DNA2* and *EXO1* is not clear, but our results suggest that the genetic lethality does not stem from a loss of Dna2 nuclease activity as this is abrogated in *dna2*-1.

Synthetic lethality of *sae2*Δ *sgs1*Δ is supressed by *NEJ1* deletion

Nej1 suppression of *sae2*Δ *sgs1*Δ synthetic lethality was dependent on Dna2, but not Exo1 nuclease activity (Fig 5F and S4) [22]. Surprisingly, the rate of 5' resection in *sae2*Δ *sgs1*Δ *nej1*Δ triple mutants were similar to wild type, and above *sae2*Δ *nej1*Δ (Fig 5D). We previously showed that both Sgs1 and Dna2 interact directly with Mre11 [4], thus in *sae2*Δ mutants the presence of Sgs1 could inhibit the initiation of resection. More specifically, Dna2-Mre11 might function to initiate resection in *sae2*Δ, with Dna2-Sgs1 being less optimal for initiating, but better in long-range resection. Deletion of *KU70* or *RAD9*, like *NEJ1*, suppresses *sae2*Δ *sgs1*Δ lethality. Moreover, the rate of 5' resection in triple mutant combinations with *ku70*Δ and *rad9*Δ, like *sae2*Δ *sgs1*Δ *nej1*Δ mutants, was similar to wild type. This rescue might result from a decrease in overall NHEJ at the DSB, however, two results suggest that the loss of end-joining itself does not rescue the lethality of *sae2*Δ *sgs1*Δ. First, deletion of *DNL4* ligase does not rescue *sae2*Δ *sgs1*Δ and second, NHEJ occurs in *sae2*Δ *sgs1*Δ *rad9*Δ triple mutants. Taken together, these data ascribe a wider range of functionality for Nej1 beyond NHEJ. Underscoring its evolutionary conservation from yeast to humans, these data provide new information about how Nej1 functions with HR nucleases at DSBs to preserve genome integrity during repair pathway choice.

Methods

Key Resource Table

REAGENT or RESOURCE	SOURCE	IDENTIFIER
Antibodies		
HA-probe mouse monoclonal antibody	Santa Cruz Biotechnology	F-7
LexA-Probe mouse monoclonal antibody	Santa Cruz Biotechnology	2-12
Myc-Probe mouse monoclonal antibody	Abcam	ab32
Peroxidase conjugated AffiniPure Goat anti-Mouse antibody	Jackson ImmunoResearch	115035174
Chemicals		
Adenine	Sigma	A8626
Bacto™ Peptone	BD Biosciences	211677
Bacto™ Yeast extract	BD Biosciences	212750
Complete EDTA free protease inhibitor cocktail	Roche	04693159001
Dextrose	Sigma	D1912
Difco™ Agar	BD Biosciences	214530
Dynabeads Sheep anti-Mouse IgG	Invitrogen	20230531
EDTA	VWR	0322
Ethanol	Commercial alcohols	P006EAAN
Formaldehyde	Sigma	F8775
Galactose	Sigma	G0750
Glycine	VWR	CA93291
Glycogen	Roche	10901393001
Lactic acid	Sigma	69785
Lithium Chloride	EMD Millipore	LX03311
Phenol-Chloroform-Isoamylalcohol	Invitrogen	15593049
PMSF	Sigma	78830
Potassium Chloride	EMD Chemicals	1049360500
Raffinose	US Biological	R1030

SDS	Avantor	409502
Sodium Acetate	VWR	BDH9278
Sodium Chloride	Fisher Chemical	S64212
Tris base	Fisher Chemical	BP1525
Triton	Sigma	9002931
Zirconia Silica beads	BioSpec Products	11079105z
Enzymes		
Proteinase K	Invitrogen	25530031
RNase A	Sigma	R6513
RsaI	New England Biolabs	R0167S
Kits		
PerfeCTa qPCR SuperMix, ROX	Quanta BioSciences Inc.	89168-786
PowerUp SYBR Green Master Mix	Applied Biosystems	A25743
Western Lightning Plus-ECL	PerkinElmer	NEL105001EA
Plasmids		
Plasmids used in this study	Table S3	
Primers		
Primers used in this study	Table S4	
Yeast strains		
Yeast strains used in this study	Table S2	

All the yeast strains used in this study are listed in Table S2 and were obtained by crosses. The strains were grown on various media in experiments described below. For HO-induction of a DSB, YPLG media is used (1% yeast extract, 2% bactopeptone, 2% lactic acid, 3% glycerol and 0.05% glucose). For the continuous DSB assay, YPA plates are used (1% yeast extract, 2% bacto peptone, 0.0025% adenine) supplemented with either 2% glucose or 2% galactose. For the mating type assays, YPAD plates are used (1% yeast extract, 2% bacto peptone, 0.0025% adenine, 2% dextrose). For yeast 2-hybrid assays, standard amino acid drop-out media lacking

histidine, tryptophan and uracil is used and 2% raffinose is added as the carbon source for the cells.

Method Details

Chromatin Immunoprecipitation

ChIP assay was performed as described previously [4]. Cells were cultured overnight in YPLG at 25°C. Cells were then diluted to equal levels (5 x 10^6 cells/ml) and were cultured to one doubling (3-4 hrs) at 30°C. 2% GAL was added to the YPLG and cells were harvested and crosslinked at various time points using 3.7% formaldehyde solution. Following crosslinking, the cells were washed with ice cold PBS and the pellet stored at -80°C. The pellet was re-suspended in lysis buffer (50mM Hepes pH 7.5, 1mM EDTA, 80mM NaCl, 1% Triton, 1mM PMSF and protease inhibitor cocktail) and cells were lysed using Zirconia beads and a bead beater. Chromatin fractionation was performed to enhance the chromatin bound nuclear fraction by spinning the cell lysate at 13,200rpm for 15 minutes and discarding the supernatant. The pellet was re-suspended in lysis buffer and sonicated to yield DNA fragments (~500bps in length). The sonicated lysate was then incubated in beads + anti-HA/Myc Antibody or unconjugated beads (control) for 2 hrs at 4°C. The beads were washed using wash buffer (100mM Tris pH 8, 250mM LiCl, 150mM (HA Ab) or 500mM (Myc Ab) NaCl, 0.5% NP-40, 1mM EDTA, 1mM PMSF and protease inhibitor cocktail) and protein-DNA complex was eluted by reverse crosslinking using 1%SDS in TE buffer, followed by proteinase K treatment and DNA isolation via phenol-chloroform-isoamyl alcohol extraction. Quantitative PCR was performed using the Applied Biosystem QuantStudio 6 Flex machine. PerfeCTa qPCR SuperMix, ROX was used to visualize enrichment at HO2 (0.5kb from DSB) and HO1 (1.6kb from DSB) and SMC2 was used as an internal control.

Tethering Microscopy

Cells derived from the parent strain JC-4066 were diluted and grown overnight in YPLG at 25°C to reach a concentration of $1x10^7$ cells/ml. Cells were treated with 2% GAL for 2 hours and cell pellets were collected and washed 2 times with PBS. After the final wash, cells were placed on cover slips and imaged using a fully motorized Nikon Ti Eclipse inverted epi-fluorescence microscope. Z-stack images were acquired with 200 nm increments along the z plane, using a 60X oil immersion 1.4 N.A. objective. Images were captured with a Hamamatsu Orca flash 4.0 v2 sCMOS 16-bit camera and the system was controlled by Nikon NIS-Element Imaging Software (Version 5.00). All images were deconvolved with Huygens Essential version 18.10 (Scientific Volume Imaging, The Netherlands, http://svi.nl), using the Classic Maximum Likelihood Estimation (CMLE) algorithm, with SNR:40 and 50 iterations. To measure the distance between the GFP and mCherry foci, the ImageJ plug-in Distance Analysis (DiAna) was used [51]. Distance measurements represent the shortest distance between the brightest pixel in the mCherry channel and the GFP channel. Each cell was measured individually and > 50 cells were analyzed per condition per biological replicate.

qPCR based Resection Assay

Cells from each strain were grown overnight in 15ml YPLG to reach an exponentially growing culture of $1x10^7$ cells/mL. Next, 2.5mL of the cells were pelleted as timepoint 0 sample, and 2% GAL was added to the remaining cells, to induce a DSB. Following that, respective timepoint samples were collected. Genomic DNA was purified using standard genomic preparation method by isopropanol precipitation and ethanol washing, and DNA was re-suspended in 100mL ddH_2O. Genomic DNA was treated with 0.005µg/µL RNase A for 45min at 37°C. 2µL of DNA was added to tubes containing CutSmart buffer with or without RsaI restriction enzyme and incubated at 37°C for 2hrs. Quantitative PCR was performed using the Applied Biosystem QuantStudio 6 Flex machine. PowerUp SYBR Green Master Mix was used to quantify resection at MAT1 (0.15kb from DSB) locus. Pre1 was used as a negative control. RsaI cut DNA was normalized to uncut DNA as previously described to quantify the %ssDNA / total DNA [35].

Continuous DSB assay and identification of mutations in survivors

Cells were grown overnight in YPLG media at 25°C to saturation. Cells were collected by centrifugation at 2500rpm for 3 minutes and pellets were washed 1x in ddH_2O and re-suspended in ddH_2O. Cells were counted and spread on YPA plates supplemented with either 2% GLU or 2% GAL. On the Glucose plates $1x10^3$ total cells were added and on the galactose plates $1x10^5$ total cells were added. The cells were incubated for 3-4 days at room temperature and colonies counted on each plate. Survival was determined by normalizing the number of surviving colonies in the GAL plates to number of colonies in the GLU plates. 100 survivors from each strain were scored for the mating type assay as previously described [9].

Yeast 2-hybrid

Various plasmids (Table S3) were constructed containing the gene encoding the region of the proteins – Sae2, Dna2, Mre11, Nej1, Rad50 and Xrs2, using the primers listed in Table S4. The plasmids J-965 and J-1493 and the inserts were treated with BamHI and EcoRI and ligated using T4 DNA ligase. The plasmids were sequence verified. Reporter (J-359), bait (J-965) and prey (J-1493) plasmids, containing the gene encoding the desired protein under a galactose inducible promoter, were transformed into JC-1280. Cells were grown overnight in –URA –HIS –TRP media with 2% raffinose. Next day, cells were transferred into –URA –HIS –TRP media with either 2% GLU or 2% GAL and grown for 6 hrs at 30°C. Cell pellets were resuspended and then permeabilized using 0.1% SDS followed by ONPG addition. β-galactosidase activity was estimated by measuring the OD at 420nm, relative β-galactosidase units were determined by normalizing to total cell density at OD600. Additionally, for drop assay cells were grown and spotted in five-fold serial dilutions on plates containing 2% galactose lacking histidine and tryptophan (for plasmid selection) and leucine (for measuring expression from *lexAop6-LEU2*). Plates were photographed after 3-4 days of incubation at 30°C.

Western Blots

Cells were lysed by re-suspending them in lysis buffer (with PMSF and protease inhibitor cocktail tablets) followed by bead beating. The protein concentration of the whole cell extract was determined using the NanoDrop. Equal amounts of whole cell extract were added to wells of 10% polyacrylamide SDS gel. After the run, the protein were transferred to Nitrocellulose

membrane at 100V for 80mins. The membrane was Ponceau stained (which served as a loading control), followed by blocking in 10% milk-PBST for 1hour at room temperature. Respective primary antibody solution (1:1000 dilution) was added and left for overnight incubation at 4°C. The membranes were then washed with PBST and left for 1 hour with secondary antibody. Followed by washing the membranes, adding the ECL substrates and imaging them.

Tetrad Analysis

Diploids of *sae2*Δ *nej1*Δ (JC-5675) X *sgs1*Δ *nej1*Δ (JC-3885) (Figure 5A); and *sae2*Δ *sgs1*Δ *nej1*Δ (JC-5749) X *dna2*-1 (JC-5655) (Figure 5F) were sporulated. The spores (*sae2*Δ::HIS, *sgs1*Δ::NAT *nej1*Δ::KAN, *dna2*-1::TS) were checked by replica-plating on the marker plates (-HIS, +NAT, +KAN and 37°C). For analysis two-two gene segregation was observed among the tetrads. The tetrad scoring data is available with the paper.

DSB Efficiency

The efficiency of HO-cutting was measured as previously described [9]. Cells were grown in YPLG before the addition of galactose to induce expression of the HO-endonuclease, leading to DSB formation. The cells were pelleted and gDNA was prepared followed by qPCR with a primer set flanking the DSB (HO6 primers, Table S4).

Supporting information

S1 Fig. ChIP of DSB factors in various mutants

(A) Enrichment of $Sgs1^{HA}$ at DSB, at 0 and 3 hours, in wild type (JC-4135), *dna2*-1 (JC-5681) and no tag control (JC-727).

(B) Enrichment of $Nej1^{Myc}$ at DSB, at 0 and 3 hours, in wild type (JC-1687), *sae2*Δ (JC-5118), *dna2*-1 (JC-5479) and no tag control (JC-727).

(C) Enrichment of yKu70^{Myc} at DSB, at 0 and 3 hours, in wild type (JC-2271), *sae2*Δ (JC-5534), *dna2*-1 (JC-5533) and no tag control (JC-727).

(D) Enrichment of Sae2^{HA} at DSB, at 0 and 3 hours, in wild type (JC-5116), *dna2*-1 (JC-5682) and no tag control (JC-727).

(E) Enrichment of Sae2^{HA} at DSB, at 0 and 3 hours, in wild type (JC-5116), *sgs1*Δ (JC-5684), *exo1*Δ (JC-5688), *nej1*Δ (JC-5124), *sgs1*Δ *nej1*Δ (JC-5685), *exo1*Δ *nej1*Δ (JC-5686), *mre11*-3 (JC-5119), *mre11*-3 *sgs1*Δ (JC-5704), *mre11*-3 *nej1*Δ (JC-5702), *mre11*-3 *sgs1*Δ *nej1*Δ (JC-5706) and no tag control (JC-727).

All the ChIP signals were determined at 0.6kb from DSB. The fold enrichment is normalized to recovery at the SMC2 locus. For all the experiments - error bars represent the standard error of three replicates. Significance was determined using 1-tailed, unpaired Student's t test. All strains compared are marked (P<0.05*; P<0.01**; P<0.001***) unless specified with a line, strains are compared to WT.

S2 Fig. Supporting data for Yeast 2 Hybrid analysis

(A) Expression of proteins upon galactose induction. Western blots showing the similar level of expression of proteins fused to LexA and HA tag upon galactose induction in WT and *nej1*Δ. PGK1 was stained as a loading control.

(B) Y2H analysis of Rad50 fused to HA-AD and Mre11 fused to lexA-DBD was performed in wild type cells (JC-1280) and in isogenic cells with *nej1*Δ (JC-4556) using a quantitative β-galactosidase assay.

S3 Fig. Microscopy and end-bridging measurements in various mutants

Scatter data plot showing the tethering of DSB ends, at 0 and 2 hours, as measured by the distance between the GFP and mCherry foci in wild type (JC- 4066), *sgs1*Δ (JC-5699), *exo1*Δ (JC-5700) and *dna2*-1 (JC-5701). The Geometric mean (GM) distance for each sample is specified under respective sample data plot. Significance was determined using Kruskal-Wallis and Dunn's multiple comparison test.

S4 Fig. Tetrad analysis with Exo1

Viability and genotypes of spores derived from diploids of *sae2*Δ *sgs1*Δ *nej1*Δ (JC-5749) and *exo1*Δ *dna2*-1 (JC-5692). The spores were checked by replica-plating on the marker plates (-HIS, +NAT, +KAN and 37°C). For analysis two-two gene segregation was observed among the tetrads.

S1 Table. DSB cut efficiency and survival in various mutants.

S2 Table. S. cerevisiae strains used in this study.

S3 Table. Plasmids used in this study.

S4 Table. Primers and Probes used in this study.

S5 Table. Data sets for this study.

Acknowledgments

This work was supported by operating grants from CIHR MOP-82736; MOP-137062 and NSERC 418122 awarded to J.A.C. The authors declare that they have no conflicts of interest with the contents of this article. We acknowledge the resources provided by the Live Cell Imaging Laboratory. The Nikon Ti Eclipse inverted epi-fluorescence microscope system was purchased with funds from the International Microbiome Centre, which is supported by the Cumming School of Medicine at University of Calgary, Western Economic Diversification (WED) and Alberta Economic Development and Trade (AEDT), Canada.

Authors Contributions

A.M. and J.A.C. designed the research. A.M., and N.A. performed experiments and analyzed the data. A.M., N.A. and J.A.C wrote the manuscript.

References

1. Wu D, Topper LM, Wilson TE. Recruitment and dissociation of nonhomologous end joining proteins at a DNA double-strand break in *Saccharomyces cerevisiae*. Genetics. 2008; 178(3): 1237-1249. doi: 10.1534/genetics.107.083535.
2. Palmbos, PL., Wu, D., Daley, JM., Wilson, TE. (2008) Recruitment of *Saccharomyces cerevisiae* Dnl4-Lif1 complex to a double-strand break requires interactions with Yku80 and the Xrs2 FHA domain. Genetics. 2008; 180: 1809–1819.
3. Chen, X., Tomkinson, AE. Yeast Nej1 is a key participant in the initial end binding and final ligation steps of nonhomologous end joining. J. Biol. Chem. 2011; 286: 4931–4940.
4. Mojumdar A., Sorenson K., Hohl M., Toulouze M., Lees-Miller SP., Dubrana K., et al. Nej1 Interacts with Mre11 to Regulate Tethering and Dna2 Binding at DNA Double-Strand Breaks. Cell Rep. 2019 Aug 6; 28(6): 1564-1573.e3. doi: 10.1016/j.celrep.2019.07.018.
5. Frank-Vaillant M, Marcand S. NHEJ regulation by mating type is exercised through a novel protein, Lif2p, essential to the ligase IV pathway. Genes Dev. 2001; 15(22): 3005-3012. doi: 10.1101/gad.206801.
6. Valencia M, Bentele M, Vaze MB, Herrmann G, Kraus E, Lee SE, et al. NEJ1 controls non-homologous end joining in *Saccharomyces cerevisiae*. Nature. 2001; 414(6864): 666-669. doi: 10.1038/414666a.
7. Zhang Y, Hefferin ML, Chen L, Shim EY, Tseng HM, Kwon Y, et al. Role of Dnl4-Lif1 in nonhomologous end-joining repair complex assembly and suppression of homologous recombination. Nat Struct Mol Biol. 2007; 14(7): 639-646. doi: 10.1038/nsmb1261.
8. Mahaney BL, Lees-Miller SP, Cobb JA. The C-terminus of Nej1 is critical for nuclear localization and non-homologous end-joining. DNA Repair (Amst). 2014; 14: 9-16. doi: 10.1016/j.dnarep.2013.12.002.
9. Sorenson KS, Mahaney BL, Lees-Miller SP, Cobb JA. The non-homologous end-joining factor Nej1 inhibits resection mediated by Dna2-Sgs1 nuclease-helicase at DNA double strand breaks. J Biol Chem. 2017; 292(35): 14576-14586.
10. Hopfner KP, Karcher A, Craig L, Woo TT, Carney JP, Tainer JA. Structural biochemistry and interaction architecture of the DNA double-strand break repair Mre11 nuclease and Rad50-ATPase. Cell. 2001; 105: 473–485.
11. Wiltzius JJ, Hohl M, Fleming JC, Petrini JH. The Rad50 hook domain is a critical determinant of Mre11 complex functions. Nat Struct Mol Biol. 2005; 12(5): 403-407. doi: 10.1038/nsmb928.
12. Hohl M, Kwon Y, Galván SM, Xue X, Tous C, Aguilera A, et al. The Rad50 coiled-coil domain is indispensable for Mre11 complex functions. Nat. Struct. Mol. Biol. 2011; 18: 1124–1131.
13. Hohl M, Kochańczyk T, Tous C, Aguilera A, Krężel A, Petrini JH. Interdependence of the rad50 hook and globular domain functions. Mol. Cell. 2015; 57: 479–491.

14. Symington LS. Mechanism and regulation of DNA end resection in eukaryotes. Crit Rev Biochem Mol Biol. 2016; 51(3): 195-212. doi: 10.3109/10409238.2016.1172552.
15. Cannavo E, Cejka P. Sae2 promotes dsDNA endonuclease activity within Mre11-Rad50-Xrs2 to resect DNA breaks. Nature. 2014; 514: 122–125.
16. Cejka P. DNA End Resection: Nucleases Team Up with the Right Partners to Initiate Homologous Recombination. J Biol Chem. 2015; 290(38): 22931-22938. doi: 10.1074/jbc.R115.675942.
17. Zhu Z, Chung WH, Shim EY, Lee SE, Ira G. Sgs1 helicase and two nucleases Dna2 and Exo1 resect DNA double-strand break ends. Cell. 2008; 134: 981–994.
18. Mimitou EP, Symington LS. Sae2, Exo1 and Sgs1 collaborate in DNA double-strand break processing. Nature 2008; 455: 770-774.
19. Shim EY, Chung WH, Nicolette ML, Zhang Y, Davis M, Zhu Z, et al. *Saccharomyces cerevisiae* Mre11/Rad50/Xrs2 and Ku proteins regulate association of Exo1 and Dna2 with DNA breaks. EMBO J. 2010; 29(19): 3370-3380. doi: 10.1038/emboj.2010.219.
20. Mimitou EP, Symington LS. Ku prevents Exo1 and Sgs1-dependent resection of DNA ends in the absence of a functional MRX complex or Sae2. EMBO J. 2010; 29(19): 3358-69.
21. Gobbini E, Villa M, Gnugnoli M, Menin L, Clerici M, Longhese MP. Sae2 Function at DNA Double-Strand Breaks Is Bypassed by Dampening Tel1 or Rad53 Activity. PLoS Genet. 2015; 11(11): e1005685. https://doi.org/10.1371/journal.pgen.1005685.
22. Yu TY, Kimble MT, Symington LS. Sae2 antagonizes Rad9 accumulation at DNA double-strand breaks to attenuate checkpoint signaling and facilitate end resection. Proc Natl Acad Sci U S A. 2018; 115(51): E11961-E11969. doi: 10.1073/pnas.1816539115.
23. Arora S, Deshpande RA, Budd M, Campbell J, Revere A, Zhang X, et al. Genetic Separation of Sae2 Nuclease Activity from Mre11 Nuclease Functions in Budding Yeast. Mol Cell Biol. 2017; 37(24): e00156-17. doi: 10.1128/MCB.00156-17.
24. Budd ME, Campbell JL. Interplay of Mre11 nuclease with Dna2 plus Sgs1 in Rad51-dependent recombinational repair. PLoS One. 2009; 4(1): e4267. doi: 10.1371/journal.pone.0004267.
25. Budd ME, Campbell JL. A new yeast gene required for DNA replication encodes a protein with homology to DNA helicases. Proc Natl Acad Sci U S A. 1995; 92(17): 7642-7646. doi:10.1073/pnas.92.17.7642.
26. Budd ME, Choe WC, Campbell JL. The nuclease activity of the yeast DNA2 protein, which is related to the RecB-like nucleases, is essential in vivo. J Biol Chem. 2000; 275(22): 16518-16529. doi: 10.1074/jbc.M909511199.
27. Jia PP, Junaid M, Ma YB, Ahmad F, Jia YF, Li WG, et al. Role of human DNA2 (hDNA2) as a potential target for cancer and other diseases: A systematic review. DNA Repair (Amst). 2017; 59: 9-19. doi: 10.1016/j.dnarep.2017.09.001.
28. Kumar S, Peng X, Daley J, Yang L, Shen J, Nguyen N, et al. Inhibition of DNA2 nuclease as a therapeutic strategy targeting replication stress in cancer cells. Oncogenesis. 2017; 6: e319. https://doi.org/10.1038/oncsis.2017.15.

29. Bae SH, Bae KH, Kim JA, Seo YS. RPA governs endonuclease switching during processing of Okazaki fragments in eukaryotes. Nature. 2001; 412(6845): 456-61. doi: 10.1038/35086609.
30. Budd ME, Reis CC, Smith S, Myung K, Campbell JL. Evidence suggesting that Pif1 helicase functions in DNA replication with the Dna2 helicase/nuclease and DNA polymerase delta. Mol Cell Biol. 2006; 26(7): 2490-500. doi: 10.1128/MCB.26.7.2490-2500.2006.
31. Bae SH, Choi E, Lee KH, Park JS, Lee SH, Seo YS. Dna2 of *Saccharomyces cerevisiae* possesses a single-stranded DNA-specific endonuclease activity that is able to act on double-stranded DNA in the presence of ATP. J Biol Chem. 1998; 273(41): 26880-90. doi: 10.1074/jbc.273.41.26880.
32. Budd ME, Campbell JL. The pattern of sensitivity of yeast dna2 mutants to DNA damaging agents suggests a role in DSB and postreplication repair pathways. Mutat Res. 2000; 459(3): 173-86. doi: 10.1016/s0921-8777(99)00072-5.
33. Daley JM, Jimenez-Sainz J, Wang W, Miller AS, Xue X, Nguyen KA, et al. Enhancement of BLM-DNA2-Mediated Long-Range DNA End Resection by CtIP. Cell Rep. 2017; 21(2): 324-332. doi: 10.1016/j.celrep.2017.09.048.
34. Ceppi I, Howard SM, Kasaciunaite K, Pinto C, Anand R, Seidel R, et al. CtIP promotes the motor activity of DNA2 to accelerate long-range DNA end resection. Proc Natl Acad Sci U S A. 2020; 117(16): 8859-8869. doi: 10.1073/pnas.2001165117.
35. Ferrari M, Dibitetto D, De Gregorio G, Eapen VV, Rawal CC, Lazzaro F, et al. Functional interplay between the 53BP1-ortholog Rad9 and the Mre11 complex regulates resection, end-tethering and repair of a double-strand break. PLoS Genet. 2015; 11(1): e1004928. doi: 10.1371/journal.pgen.1004928.
36. Öz R, Howard SM, Sharma R, Törnkvist H, Ceppi I, Kk S, et al. Phosphorylated CtIP bridges DNA to promote annealing of broken ends. Proc Natl Acad Sci U S A. 2020; 117(35): 21403-21412. doi: 10.1073/pnas.2008645117.
37. Andres SN, Li ZM, Erie DA, Williams RS. Ctp1 protein-DNA filaments promote DNA bridging and DNA double-strand break repair. J Biol Chem. 2019; 294(9): 3312-3320. doi: 10.1074/jbc.RA118.006759.
38. Hohl M, Mojumdar A, Hailemariam S, Kuryavyi V, Ghisays F, Sorenson K, et al. Modeling cancer genomic data in yeast reveals selection against ATM function during tumorigenesis. PLoS Genet. 2020; 16(3): e1008422. doi: 10.1371/journal.pgen.1008422.
39. Moore JK, Haber JE. Cell cycle and genetic requirements of two pathways of nonhomologous end-joining repair of double-strand breaks in *Saccharomyces cerevisiae*. Mol. Cell. Biol. 1996; 16: 2164–2173.
40. Bressan DA, Olivares HA, Nelms BE, Petrini JH. Alteration of N-terminal phosphoesterase signature motifs inactivates *Saccharomyces cerevisiae* Mre11. Genetics 1998; 150: 591–600.
41. Foster SS, Balestrini A, Petrini JH. Functional interplay of the Mre11 nuclease and Ku in the response to replication-associated DNA damage. Mol Cell Biol. 2011; 31(21): 4379-89. doi: 10.1128/MCB.05854-11.

42. Bustard D, Menolfi D, Jeppsson K, Ball LG, Dewey SC, Shirahige K, et al. During replication stress Non-Smc-Element 5 is required for Smc5/6 complex functionality at stalled forks. J Biol Chem. 2012; 287: 11374-11383.
43. Cannavo E, Johnson D, Andres SN, Kissling VM, Reinert JK, Garcia V, et al. Regulatory control of DNA end resection by Sae2 phosphorylation. Nat Commun. 2018; 9(1): 4016. doi: 10.1038/s41467-018-06417-5.
44. Langerak P, Mejia-Ramirez E, Limbo O, Russell P. Release of Ku and MRN from DNA ends by Mre11 nuclease activity and Ctp1 is required for homologous recombination repair of double-strand breaks. PLoS Genet. 2011; 7(9): e1002271. doi: 10.1371/journal.pgen.1002271.
45. Hoa NN, Kobayashi J, Omura M, Hirakawa M, Yang SH, Komatsu K, Paull TT, Takeda S, Sasanuma H. BRCA1 and CtIP Are Both Required to Recruit Dna2 at Double-Strand Breaks in Homologous Recombination. PLoS One. 2015; 10(4): e0124495. doi: 10.1371/journal.pone.0124495.
46. Kim HS, Vijayakumar S, Reger M, Harrison JC, Haber JE, Weil C, et al. Functional interactions between Sae2 and the Mre11 complex. Genetics. 2008; 178(2): 711-723. doi: 10.1534/genetics.107.081331.
47. Fu Q, Chow J, Bernstein KA, Makharashvili N, Arora S, Lee CF, et al. Phosphorylation-regulated transitions in an oligomeric state control the activity of the Sae2 DNA repair enzyme. Mol Cell Biol. 2014; 34(5): 778-793. doi: 10.1128/MCB.00963-13.
48. Lobachev K, Vitriol E, Stemple J, Resnick MA, Bloom K. Chromosome fragmentation after induction of a double-strand break is an active process prevented by the RMX repair *complex. Curr Biol. 2004*; 14(23): 2107-12.
49. Bonetti D, Villa M, Gobbini E, Cassani C, Tedeschi G, Longhese MP. Escape of Sgs1 from Rad9 inhibition reduces the requirement for Sae2 and functional MRX in DNA end resection. EMBO Rep. 2015; 16(3): 351-61. doi: 10.15252/embr.201439764.
50. Kumar S, Burgers PM. Lagging strand maturation factor Dna2 is a component of the replication checkpoint initiation machinery. Genes Dev. 2013; 27(3): 313-21. doi: 10.1101/gad.204750.112.
51. Gilles JF, Dos Santos M, Boudier T, Bolte S, Heck N. DiAna, an ImageJ tool for object-based 3D co-localization and distance analysis. Methods. 2017; 115: 55-64. doi: 10.1016/j.ymeth.2016.11.016.

Figure Legends

Fig 1. Sgs1-independent recruitment of Dna2 nuclease is inhibited by Nej1 at DSB.

(A) Schematic representation of regions around the HO cut site on chromosome III. The ChIP probe used in this study is 0.6kb from the DSB. The RsaI sites used in the qPCR resection assays, 0.15kb from the DSB, are also indicated. Both sides of HO cut site are tagged with GFP (5kb from cute site) and mCherry (9kb from cut site) repeats, which were used in end-tethering microscopy.

(B) qPCR-based resection assay of DNA 0.15kb away from the HO DSB, as measured by % ssDNA, at 0, 40, 80 and 150 min post DSB induction in cycling cells in wild type (JC-727), *nej1*Δ (JC-1342), *sgs1*Δ (JC-3757), *sgs1*Δ *nej1*Δ (JC-3759), *dna2*-1 (JC-5655), *dna2*-1 *nej1*Δ (JC-5670), *dna2*-1 *sgs1*Δ (JC-5745) and *dna2*-1 *sgs1*Δ *nej1*Δ (JC-5746).

(C) Enrichment of $Dna2^{HA}$ at 0.6kb from DSB 0 hour (no DSB induction) and 3 hours after DSB induction in wild type (JC-4117), *nej1*Δ (JC-4118), *sgs1*Δ (JC-5624), *dna2*-1 (JC-5707), *sgs1*Δ *nej1*Δ (JC-5627) and no tag control (JC-727) was determined. The fold enrichment is normalized to recovery at the SMC2 locus.

(D) Percentage cell survival upon chronic HO induction in cells mentioned in (B).

(E) Schematic representation of mating type analysis of survivors from persistent DSB induction assays. The mating phenotype is a read out for the type of repair: α survivors (mutated HO endonuclease-site, grey), sterile survivors (small insertions and deletions, blue) and "a-like" survivors (>700 bps deletion, red).

(F) Mating type analysis of survivors from persistent DSB induction assays mentioned in (D).

For all the experiments - error bars represent the standard error of three replicates. Significance was determined using 1-tailed, unpaired Student's t test. All strains compared are marked (P<0.05*; P<0.01**; P<0.001***) and are compared to WT, unless specified with a line.

Fig 2. Dna2 recruitment to DSB is independent of Exo1.

(A) qPCR-based resection assay of DNA 0.15kb away from the HO DSB, as measured by % ssDNA, at 0, 40, 80 and 150 min post DSB induction in cycling cells in wild type (JC-727), *nej1*Δ (JC-1342), *mre11*-3 (JC-5372), *mre11*-3 *nej1*Δ (JC-5369), *mre11*-3 *sgs1*Δ (JC-5405), *mre11*-3 *sgs1*Δ *nej1*Δ (JC-5667), *mre11*-3 *dna2*-1 (JC-5748) and *mre11*-3 *dna2*-1 *nej1*Δ (JC-5532).

(B) qPCR based resection assay of DNA 0.15kb away from the HO DSB, as measured by % ssDNA, at 0, 40, 80 and 150 min post DSB induction in cycling cells in wild type (JC-727), *nej1*Δ

(JC-1342), *exo1*Δ (JC-3767), *exo1*Δ *nej1*Δ (JC-5373), *exo1*Δ *sgs1*Δ (JC-4520), *exo1*Δ *sgs1*Δ *nej1*Δ (JC-5493), *exo1*Δ *dna2*-1 (JC-5692) and *exo1*Δ *dna2*-1 *nej1*Δ (JC-5630).

(C) Percentage cell survival upon chronic HO induction in cells mentioned in (A and B).

(D) Mating type analysis of survivors from persistent DSB induction assays mentioned in (A and B).

(E) Enrichment of Dna2^{HA} at 0.6kb from DSB 0 hour (no DSB induction) and 3 hours after DSB induction in wild type (JC-4117), *nej1*Δ (JC-4118), *mre11*-3 (JC-5594), *mre11*-3 *nej1*Δ (JC-5596), *mre11*-3 *sgs1*Δ (JC-5621), *mre11*-3 *sgs1*Δ *nej1*Δ (JC-5623), *exo1*Δ (JC-5626), *exo1*Δ *nej1*Δ (JC-5666), *exo1*Δ *sgs1*Δ (JC-5559), *exo1*Δ *sgs1*Δ *nej1*Δ (JC-5566) and no tag control (JC-727) was determined. The fold enrichment is normalized to recovery at the SMC2 locus.

For all the experiments - error bars represent the standard error of three replicates. Significance was determined using 1-tailed, unpaired Student's t test. All strains compared are marked (P<0.05*; P<0.01**; P<0.001***) and are compared to WT, unless specified with a line.

Fig 3. Sae2-dependent recruitment of Dna2 is inhibited by Nej1.

(A) Enrichment of Sae2^{HA} at 0.6kb from DSB 0 hour (no DSB induction) and 3 hours after DSB induction in wild type (JC-5116), *mre11*Δ (JC-5122), *mre11*-3 (JC-5119), *nej1*Δ (JC-5124), *mre11*-3 *nej1*Δ (JC-5702) and no tag control (JC-727). The fold enrichment represents normalization over the SMC2 locus.

(B) Enrichment of Dna2^{HA} at 0.6kb from DSB 0 hour (no DSB induction) and 3 hours after DSB induction in wild type (JC-4117), *nej1*Δ (JC-4118), *sae2*Δ (JC-5562), *sae2*Δ *nej1*Δ (JC-5597), *sae2*Δ *mre11*-3 (JC-5598), *sae2*Δ *mre11*-3 *nej1*Δ (JC-5593) and no tag control (JC-727) was determined. The fold enrichment is normalized to recovery at the SMC2 locus.

(C) qPCR-based resection assay of DNA 0.15kb away from the HO DSB, as measured by % ssDNA, at 0, 40, 80 and 150 min post DSB induction in cycling cells in wild type (JC-727), *nej1*Δ (JC-1342), *sae2*Δ (JC-5673), *sae2*Δ *nej1*Δ (JC-5675), *sae2*Δ *mre11*-3 (JC-5501), *sae2*Δ *mre11*-3 *nej1*Δ (JC-5500), *sae2*Δ *dna2*-1 (JC-5669) and *sae2*Δ *dna2*-1 *nej1*Δ (JC-5671).

(D) Y2H analysis of Sae2 fused to HA-AD and Mre11, Rad50, Xrs2, Nej1 and domains of Dna2, (Dna2-N terminal, Dna2-Nuclease and Dna2-Helicase domains) fused to lexA-DBD was performed in wild type cells (JC-1280) and in isogenic cells with *nej1*Δ (JC-4556) using a quantitative β-galactosidase assay and a drop assay on drop-out (-His, -Trp, -Leu) selective media plates.

For all the experiments - error bars represent the standard error of three replicates. Significance was determined using 1-tailed, unpaired Student's t test. All strains compared are marked (P<0.05*; P<0.01**; P<0.001***) and are compared to WT, unless specified with a line.

Fig 4. Nej1-Sae2 plays a role in end-bridging at DSB.

(A) Percentage cell survival upon chronic HO induction in cells in wild type (JC-727), *nej1*Δ (JC-1342), *sae2*Δ (JC-5673), *sae2*Δ *nej1*Δ (JC-5675), *sae2*Δ *mre11*-3 (JC-5501), *sae2*Δ *mre11*-3 *nej1*Δ (JC-5500), *sae2*Δ *dna2*-1 (JC-5669) and *sae2*Δ *dna2*-1 *nej1*Δ (JC-5671).

(B) Mating type analysis of survivors from persistent DSB induction assays mentioned in (A).

(C) Representative image of yeast cells with tethered (co-localized GFP and mCherry) and untethered (distant GFP and mCherry) ends.

(D) Scatter plot showing the tethering of DSB ends, at 0 and 2 hours, as measured by the distance between the GFP and mCherry foci in wild type (JC- 4066), *nej1*Δ (JC-4364), *sae2*Δ (JC-5524), *sae2*Δ *nej1*Δ (JC-5525), *mre11*-3 (JC-5529), *mre11*-3 *nej1*Δ (JC-5526), *sae2*Δ *mre11*-3 (JC-5530) and *sae2*Δ *mre11*-3 *nej1*Δ (JC-5531). The Geometric mean (GM) distance for each sample is specified under the respective sample data plot. Significance was determined using Kruskal-Wallis and Dunn's multiple comparison test.

(E) Model of DSB where Nej1 inhibits the physical association of Dna2-Sae2 and prevents Sae2-dependent Dna2 recruitment. Created with BioRender.com

Fig 5. Dna2 plays a major role in resection at DSB that is inhibited by Nej1.

(A) Viability and genotypes of spores derived from diploids of *sae2*Δ *nej1*Δ (JC-5675) and *sgs1*Δ *nej1*Δ (JC-3885).

(B) Percentage cell survival upon chronic HO induction in cells in wild type (JC-727), *nej1*Δ (JC-1342), *sae2*Δ (JC-5673), *sae2*Δ *nej1*Δ (JC-5675), *sgs1*Δ (JC-3757), *sgs1*Δ *nej1*Δ (JC-3759) and *sae2*Δ *sgs1*Δ *nej1*Δ (JC-5750).

(C) Mating type analysis of survivors from persistent DSB induction assays mentioned in (B and described in 1A).

(D) qPCR-based resection assay of DNA 0.15kb away from the HO DSB, as measured by % ssDNA, at 0, 40, 80 and 150 mins. post DSB induction in cycling cells mentioned in (B).

(E) Enrichment of $Dna2^{HA}$ at 0.6kb from DSB 0 hour (no DSB induction) and 3 hours after DSB induction in wild type (JC-4117), *sae2*Δ *sgs1*Δ *nej1*Δ (JC-5480) and no tag control (JC-727) was determined. The fold enrichment is normalized to recovery at the SMC2 locus.

(F) Viability and genotypes of spores derived from diploids of *sae2*Δ *sgs1*Δ *nej1*Δ (JC-5749) and *dna2*-1 (JC-5655).

(G) Model of DSB where Nej1 prevents Mre11-dependent Dna2 recruitment to DSB. (a) In wild type cells Nej1 inhibits Dna2 recruitment via Mre11, Sae2 and Sgs1. (b) In *sae2*Δ *sgs1*Δ mutant cells Nej1 inhibits Dna2-Mre11 interaction and therefore prevents the residual Dna2 recruitment and resection, resulting into the synthetic lethality. (c) Upon *NEJ1* deletion, Dna2 can get recruited through Mre11 leading to resection and repair, resulting into alleviation of the synthetic lethality and growth of *sae2*Δ *sgs1*Δ *nej1*Δ cells. Created with BioRender.com

For all the experiments - error bars represent the standard error of three replicates. Significance was determined using 1-tailed, unpaired Student's t test. All strains compared are marked ($P<0.05$*; $P<0.01$**; $P<0.001$***) unless specified with a line, strains are compared to WT.

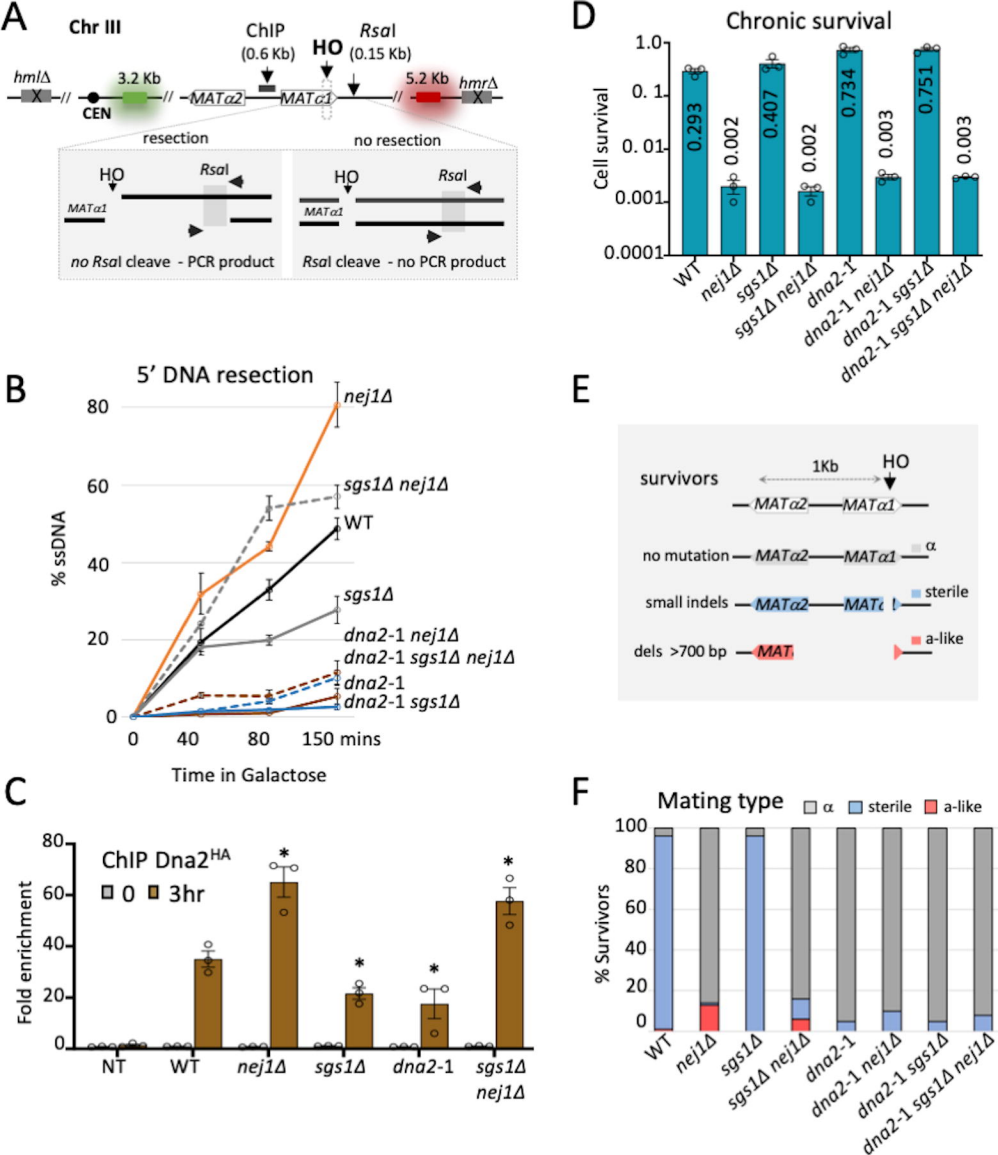
A
Chr III
ChIP
(0.6 Kb)
HO
RsaI
(0.15 Kb)
hmlΔ
3.2 Kb
CEN
MATα2
MATα1
5.2 Kb
hmrΔ
resection
no resection
HO
RsaI
MATα1
no RsaI cleave - PCR product
RsaI cleave - no PCR product
B
5' DNA resection
% ssDNA
Time in Galactose
nej1Δ
sgs1Δ nej1Δ
WT
sgs1Δ
dna2-1 nej1Δ
dna2-1 sgs1Δ nej1Δ
dna2-1
dna2-1 sgs1Δ
C
ChIP Dna2HA
0
3hr
Fold enrichment
NT
WT
nej1Δ
sgs1Δ
dna2-1
sgs1Δ nej1Δ
D
Chronic survival
Cell survival
0.293
0.002
0.407
0.002
0.734
0.003
0.751
0.003
WT
nej1Δ
sgs1Δ
sgs1Δ nej1Δ
dna2-1
dna2-1 nej1Δ
dna2-1 sgs1Δ
dna2-1 sgs1Δ nej1Δ
E
survivors
1Kb
HO
MATα2
MATα1
no mutation
α
small indels
sterile
dels >700 bp
a-like
F
Mating type
α
sterile
a-like
% Survivors
WT
nej1Δ
sgs1Δ
sgs1Δ nej1Δ
dna2-1
dna2-1 nej1Δ
dna2-1 sgs1Δ
dna2-1 sgs1Δ nej1Δ

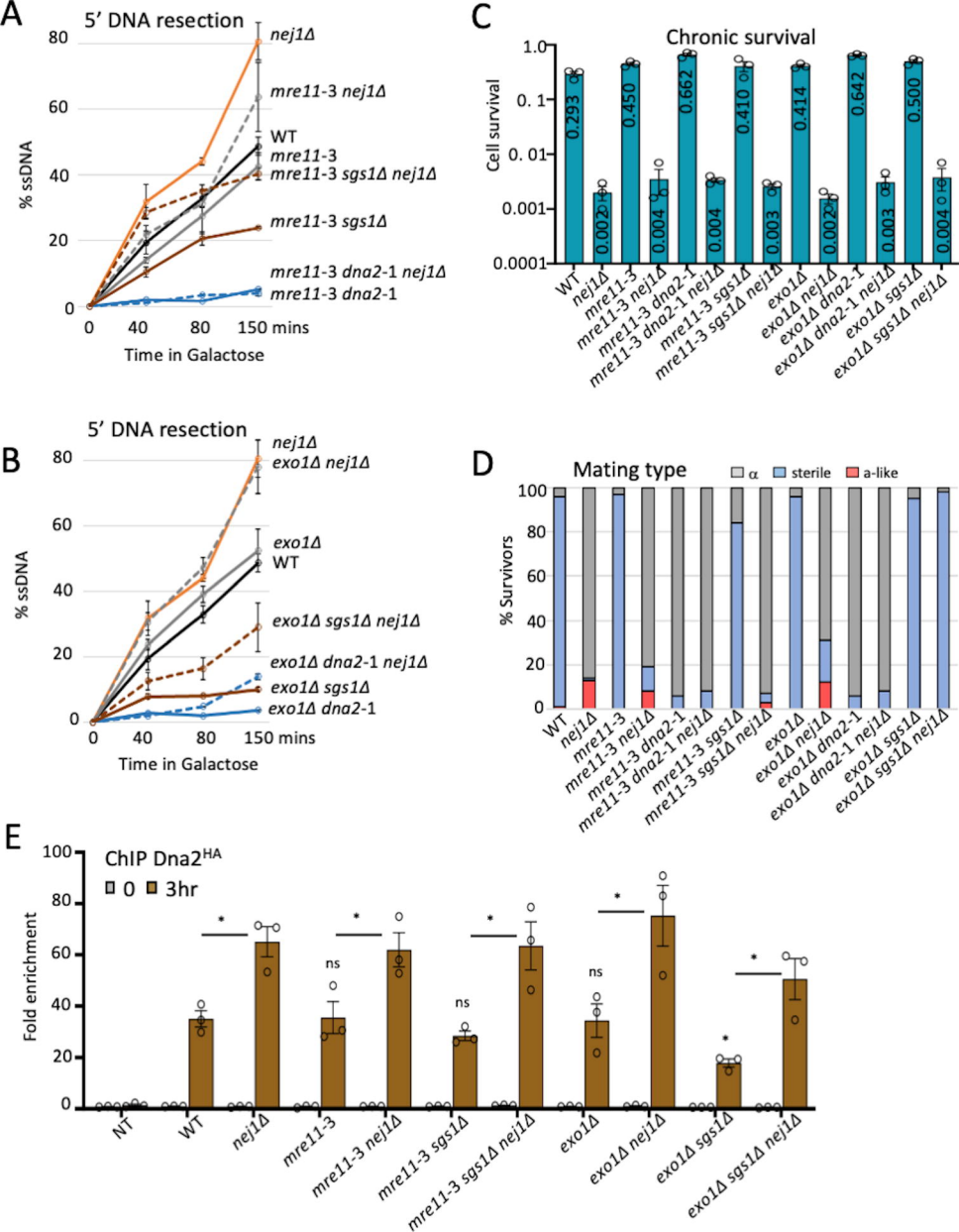
A
5' DNA resection
% ssDNA
Time in Galactose
0
40
80
150 mins
nej1Δ
mre11-3 nej1Δ
WT
mre11-3
mre11-3 sgs1Δ nej1Δ
mre11-3 sgs1Δ
mre11-3 dna2-1 nej1Δ
mre11-3 dna2-1
B
5' DNA resection
% ssDNA
Time in Galactose
nej1Δ
exo1Δ nej1Δ
exo1Δ
WT
exo1Δ sgs1Δ nej1Δ
exo1Δ dna2-1 nej1Δ
exo1Δ sgs1Δ
exo1Δ dna2-1
C
Chronic survival
Cell survival
0.293
0.002
0.450
0.004
0.662
0.004
0.410
0.003
0.414
0.002
0.642
0.003
0.500
0.004
WT
nej1Δ
mre11-3
mre11-3 nej1Δ
mre11-3 dna2-1
mre11-3 dna2-1 nej1Δ
mre11-3 sgs1Δ
mre11-3 sgs1Δ nej1Δ
exo1Δ
exo1Δ nej1Δ
exo1Δ dna2-1
exo1Δ dna2-1 nej1Δ
exo1Δ sgs1Δ
exo1Δ sgs1Δ nej1Δ
D
Mating type
α
sterile
a-like
% Survivors
E
ChIP Dna2HA
0
3hr
Fold enrichment
NT
WT
nej1Δ
mre11-3
mre11-3 nej1Δ
mre11-3 sgs1Δ
mre11-3 sgs1Δ nej1Δ
exo1Δ
exo1Δ nej1Δ
exo1Δ sgs1Δ
exo1Δ sgs1Δ nej1Δ
ns
*

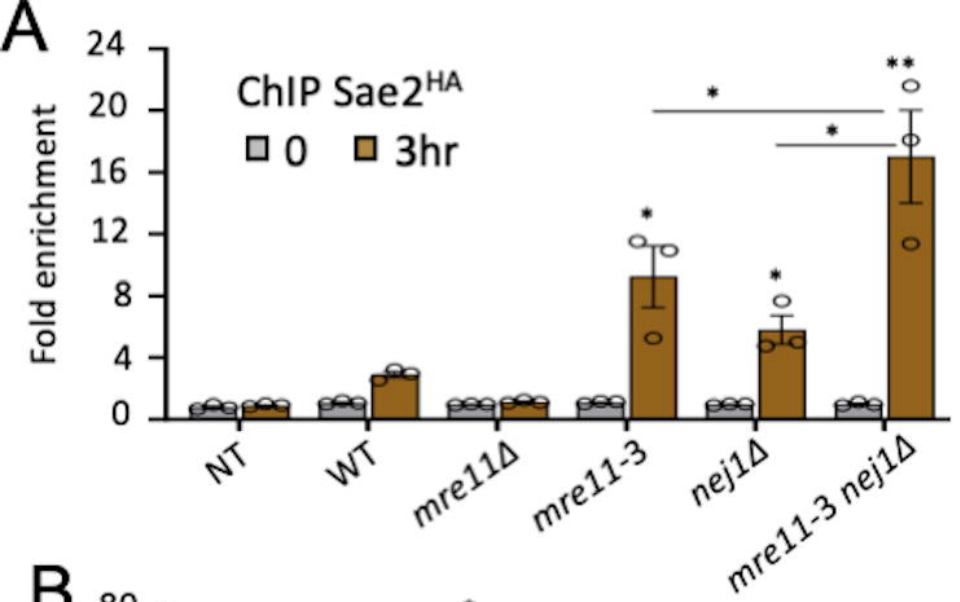
A
ChIP Sae2HA
0
3hr
Fold enrichment
24
20
16
12
8
4
0
NT
WT
mre11Δ
mre11-3
nej1Δ
mre11-3 nej1Δ

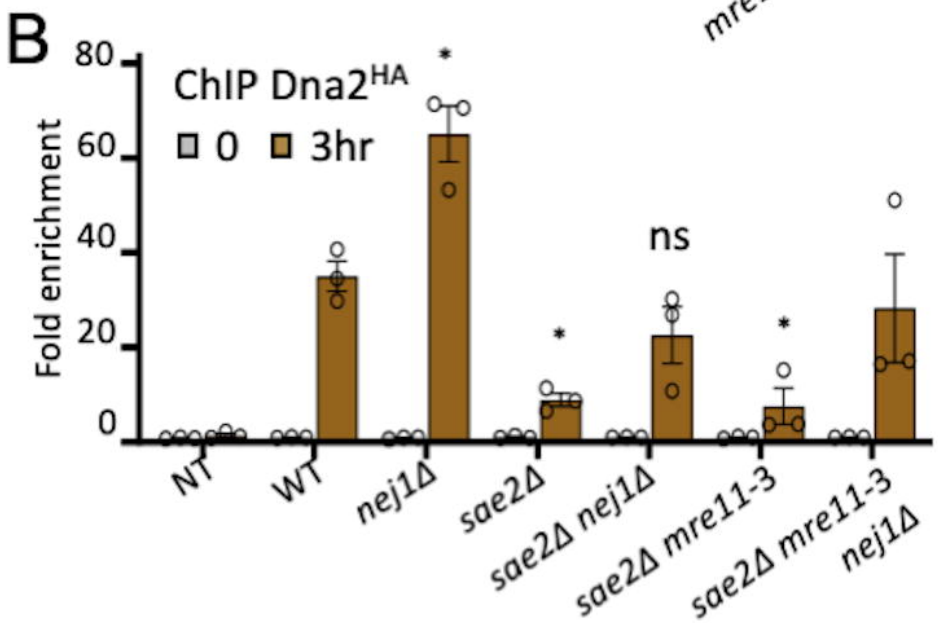
B
ChIP Dna2HA
0
3hr
Fold enrichment
80
60
40
20
0
ns
NT
WT
nej1Δ
sae2Δ
sae2Δ nej1Δ
sae2Δ mre11-3
sae2Δ mre11-3 nej1Δ

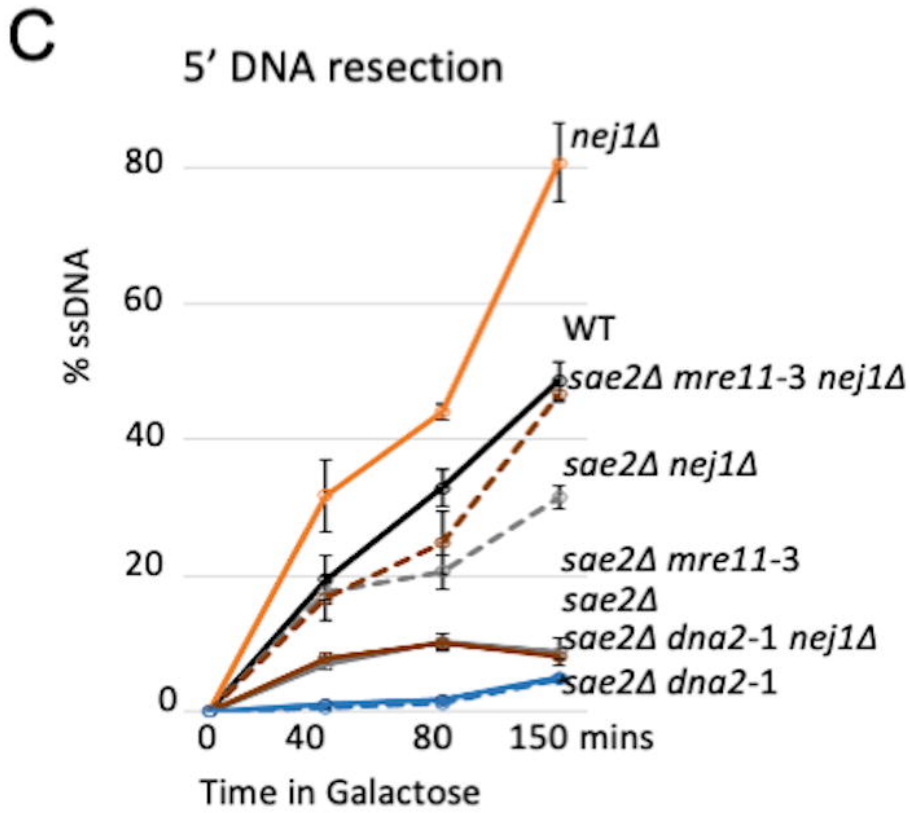
C
5' DNA resection
% ssDNA
80
60
40
20
0
nej1Δ
WT
sae2Δ mre11-3 nej1Δ
sae2Δ nej1Δ
sae2Δ mre11-3
sae2Δ
sae2Δ dna2-1 nej1Δ
sae2Δ dna2-1
0
40
80
150 mins
Time in Galactose

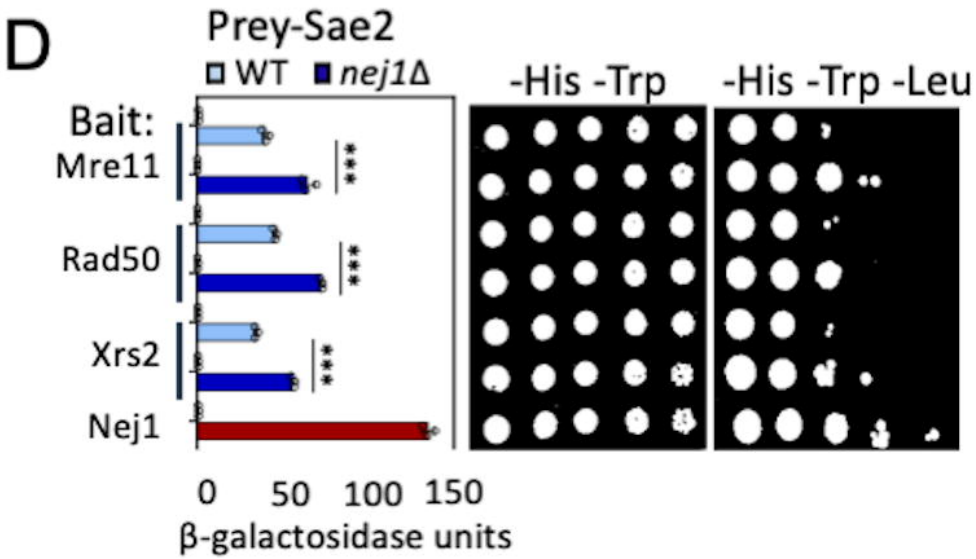
D
Prey-Sae2
WT
nej1Δ
Bait:
Mre11
Rad50
Xrs2
Nej1
-His -Trp
-His -Trp -Leu
0
50
100
150
β-galactosidase units

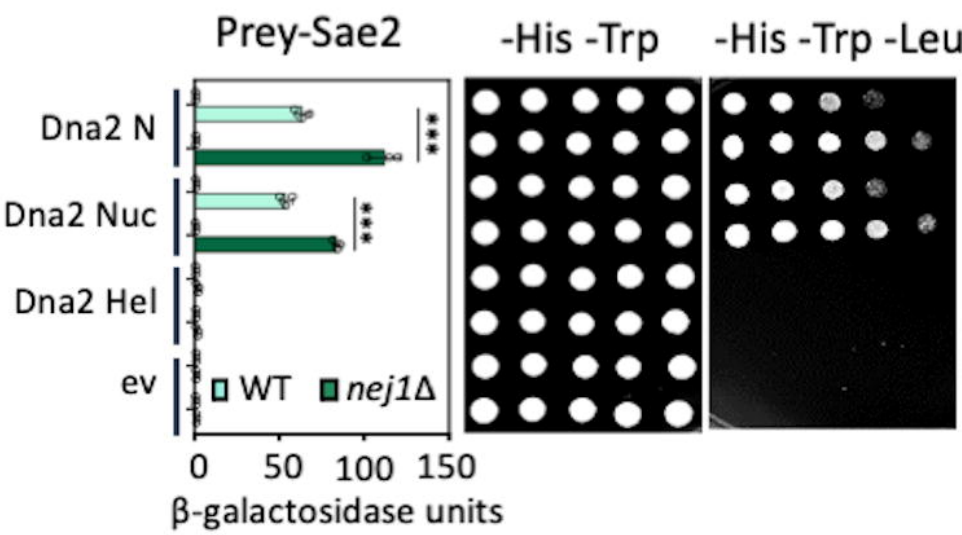
Prey-Sae2
-His -Trp
-His -Trp -Leu
Dna2 N
Dna2 Nuc
Dna2 Hel
ev
WT
nej1Δ
0
50
100
150
β-galactosidase units

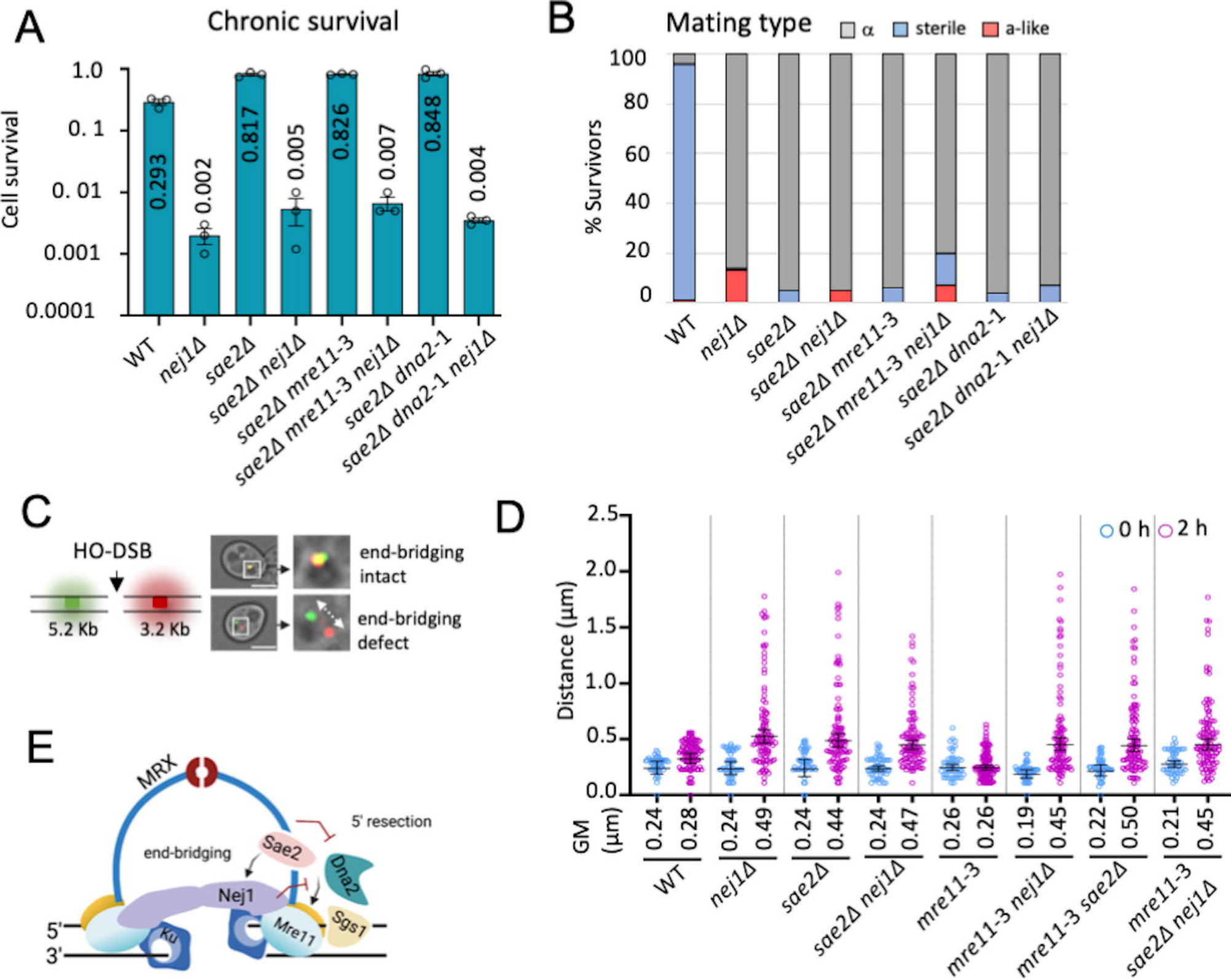
A
Chronic survival
Cell survival
1.0
0. 1
0. 01
0.001
0.0001
0.293
0.002
0.817
0.005
0.826
0.007
0.848
0.004
WT
nej1Δ
sae2Δ
sae2Δ nej1Δ
sae2Δ mre11-3
sae2Δ mre11-3 nej1Δ
sae2Δ dna2-1
sae2Δ dna2-1 nej1Δ
B
Mating type
α
sterile
a-like
% Survivors
100
80
60
40
20
0
WT
nej1Δ
sae2Δ
sae2Δ nej1Δ
sae2Δ mre11-3
sae2Δ mre11-3 nej1Δ
sae2Δ dna2-1
sae2Δ dna2-1 nej1Δ
C
HO-DSB
5.2 Kb
3.2 Kb
end-bridging intact
end-bridging defect
D
0 h
2 h
Distance (µm)
2.5
2.0
1.5
1.0
0.5
0.0
GM (µm)
0.24
0.28
0.24
0.49
0.24
0.44
0.24
0.47
0.26
0.26
0.19
0.45
0.22
0.50
0.21
0.45
WT
nej1Δ
sae2Δ
sae2Δ nej1Δ
mre11-3
mre11-3 nej1Δ
mre11-3 sae2Δ
mre11-3 sae2Δ nej1Δ
E
MRX
5' resection
end-bridging
Sae2
Dna2
Nej1
Ku
Mre11
Sgs1
5'
3'

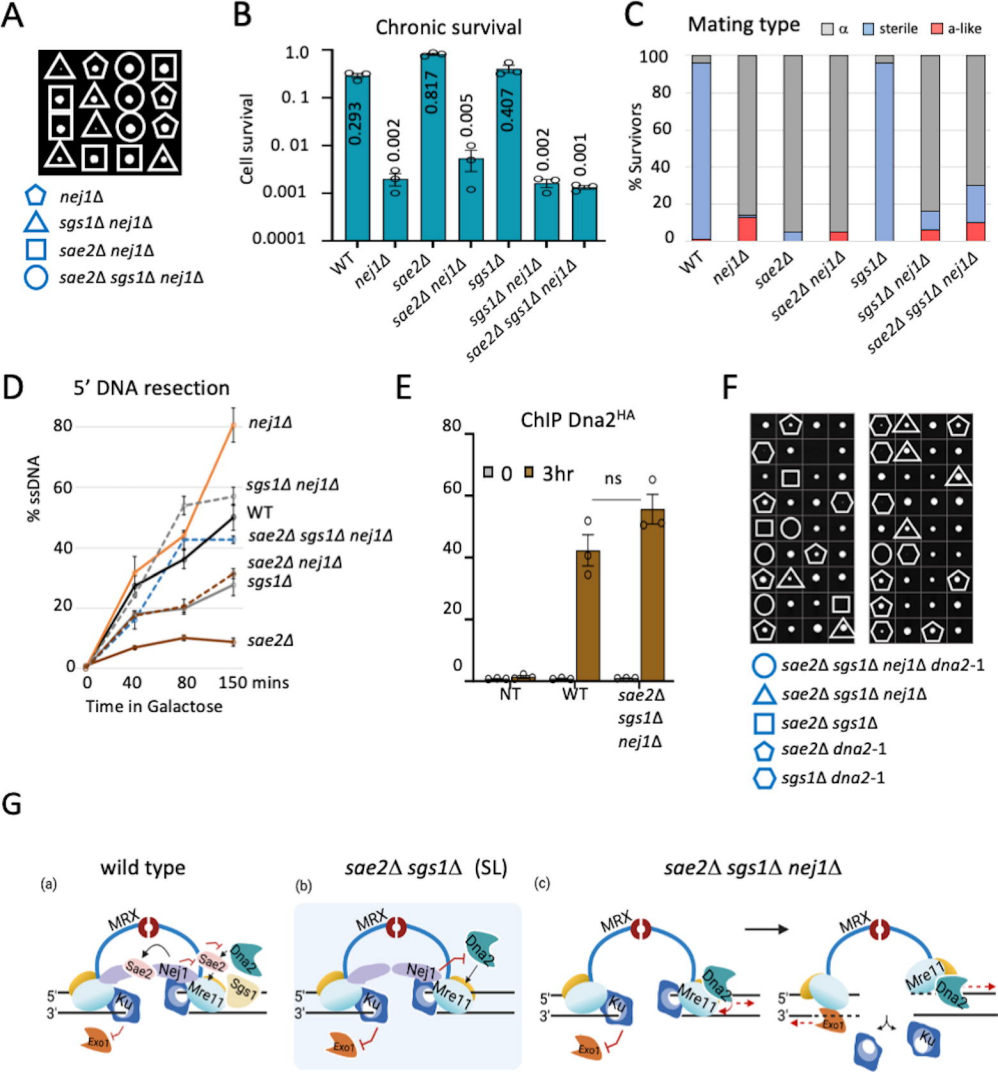
A
nej1Δ
sgs1Δ nej1Δ
sae2Δ nej1Δ
sae2Δ sgs1Δ nej1Δ
B
Chronic survival
Cell survival
1.0
0.1
0.01
0.001
0.0001
0.293
0.002
0.817
0.005
0.407
0.002
0.001
WT
nej1Δ
sae2Δ
sae2Δ nej1Δ
sgs1Δ
sgs1Δ nej1Δ
sae2Δ sgs1Δ nej1Δ
C
Mating type
α
sterile
a-like
% Survivors
100
80
60
40
20
0
WT
nej1Δ
sae2Δ
sae2Δ nej1Δ
sgs1Δ
sgs1Δ nej1Δ
sae2Δ sgs1Δ nej1Δ
D
5' DNA resection
% ssDNA
80
60
40
20
0
nej1Δ
sgs1Δ nej1Δ
WT
sae2Δ sgs1Δ nej1Δ
sae2Δ nej1Δ
sgs1Δ
sae2Δ
0
40
80
150 mins
Time in Galactose
E
ChIP Dna2HA
0
3hr
ns
80
60
40
20
0
NT
WT
sae2Δ sgs1Δ nej1Δ
F
sae2Δ sgs1Δ nej1Δ dna2-1
sae2Δ sgs1Δ nej1Δ
sae2Δ sgs1Δ
sae2Δ dna2-1
sgs1Δ dna2-1
G
wild type
sae2Δ sgs1Δ (SL)
sae2Δ sgs1Δ nej1Δ
(a)
(b)
(c)
MRX
Sae2
Nej1
Mre11
Dna2
Sgs1
Ku
Exo1
5'
3'
Mre11